

Project Title: **Center for Radiative Shock Hydrodynamics**

Project Year 2 Report

DOE Cooperative Agreement Number DE-FC52-08NA28616

Date: April 15, 2010

Period Covered: April 16, 2009 through April 15, 2010

Project Director:

R Paul Drake, Atmospheric, Oceanic and Space Sciences,
University of Michigan

Co-Principal Investigators:

Marvin L. Adams, Nuclear Engineering, Texas A & M University
James P. Holloway, Nuclear Engineering and Radiological Sciences, University of Michigan
Kenneth G. Powell, Aerospace Engineering, University of Michigan
Quentin F. Stout, Computer Science and Engineering, University of Michigan

Co-Investigators, University of Michigan:

Natasha Andronova, Atmospheric, Oceanic and Space Sciences
Krzysztof J. Fidkowski, Aerospace Engineering
Bruce Fryxell, Atmospheric, Oceanic and Space Sciences
Tamas I. Gombosi, Atmospheric, Oceanic and Space Sciences
Smadar Karni, Mathematics
Carolyn C. Kuranz, Atmospheric, Oceanic and Space Sciences
Edward W. Larsen, Nuclear Engineering and Radiological Sciences
William R. Martin, Nuclear Engineering and Radiological Sciences
Eric Myra, Atmospheric, Oceanic and Space Sciences
Vijayan Nair, Statistics
Philip I. Roe, Aerospace Engineering
Igor Sokolov, Atmospheric, Oceanic and Space Sciences
Katsuyo Thornton, Materials Science and Engineering
Ben Torralva, Materials Science and Engineerin
Gabor Toth, Atmospheric, Oceanic and Space Sciences
Bartholomeus van der Holst, Atmospheric, Oceanic and Space Sciences
Bram van Leer, Aerospace Engineering

Co-Investigators, Texas A & M University:

Nancy Amato, Computer Science
Bani Mallick, Statistics
Ryan G. McClarren, Nuclear Engineering
James E. Morel, Nuclear Engineering
Lawrence Rauchwerger, Computer Science

Co-Investigator, Simon Frazier University:

Derek Bingham, Statistics

Executive Summary

The goal of the Center for Radiative Shock Hydrodynamics (CRASH) is to develop and demonstrate methods for the Assessment of Predictive Capability (APC) of complex computer simulations, by working with simulations of radiative shock experiments performed on high-energy laser systems. The radiative shocks are driven in xenon gas by a Be plasma accelerated to > 150 km/s by laser ablation. The simulations are based on adding capability to two codes: the Block-Adaptive Tree, Solar-wind Roe-type Upwind Scheme (BATSRUS) code used extensively in space weather modeling by the University of Michigan (UM), and the Parallel Deterministic Transport (PDT) code developed initially for neutron transport calculations on massively parallel computers by Texas A&M University (TAMU).

Since being funded on April 15, 2008, CRASH released a 1.0 version of a modified BATSRUS code, and used it for initial studies to gain experience with the end-to-end process of uncertainty quantification and assessment of predictive capability. Our first assessment of predictive capability, using one-dimensional simulations, is discussed in this report. This experience with all the elements of the process now guides our planning as we move to more complete and realistic studies.

We are actively using CRASH 2.0, which includes multigroup-diffusion radiation transport, dynamic adaptive mesh refinement, and electron heat transport, completing the minimum set of physics that we expect to be needed to model our physical system. We will tag this version once our UQ studies require this. Our attention now turns primarily to improvements that are needed for more efficient operation, to sources of numerical error, to more extensive code validation. Although we had originally planned to begin integration of the higher fidelity PDT radiation transport model into the CRASH code this year, it was suggested by a member of the TST team that an integrated BATSRUS/PDT code might be UCNI. While this question is being determined, we have turned our attention to the performance of standalone CRASH and PDT calculations that will shed light on the importance of higher fidelity radiation transport for the CRASH problem..

We have also now conducted two experimental sequences, the first aimed at quantifying experimental variability and the second at calibrating the initialization of our models. We will design our next experimental sequence with substantial input from our predictive capability analysis now underway.

Our progress in all the above areas is discussed in the present report.

Training of graduate students is an important aspect of CRASH. At present, we have 21 graduate students whose research is or will be supported at least in part by the center. Three previous students completed their dissertations during the past year. These students are working on all aspects of the project, including experiments, fluid dynamics modeling, radiation transport methods, uncertainty quantification, and APC methods.

At both UM and TAMU, courses in uncertainty quantification and sensitivity analysis were introduced this year. The course at TAMU focused on verification, validation, sensitivity analysis and UQ; the course at UM focused on input/output modeling, screening and sensitivity analysis, and UQ. Both courses included homework covering basic topics, and culminated with student independent projects. More than two dozen graduate students from a wide variety of departments took the courses.

Table of Contents

Executive Summary	2
I. Project Overview	5
II. Assessment of Predictive Capability (APC)	9
A. Overview of CRASH UQ methodology	9
B. Predictive capability study using 1D simulations	11
B. Sensitivity analysis from three-dimensional simulations.....	20
C. Verification of uncertainty quantification software	22
D. 2D HYADES run set.....	25
E. Shock Morphology	27
III. Code development, verification, and testing.....	28
A. Equation of state and opacity model.....	30
B. Electron energy equation with semi-implicit heat conduction.....	31
C. Radiative transport with multigroup diffusion	33
D. Synthetic radiographs.....	35
E. Block Adaptive Tree Library.....	37
F. Run results with CRASH 2.0.....	39
G. Parallel Deterministic Transport (PDT).....	39
H. Software testing and verification: Test Matrix	43
IV. Experiments	47
V. Educational Status and Plans	50
VI. Graduate Student Research.....	51
VII. References	59

I. Project Overview

The overarching goal of the CRASH project is to use scientific methods to assess and to improve the predictive capability of a simulation code, based on a combination of physical and statistical analysis and experimental data. The specific focus of the project is radiative shocks, which develop when shock waves become so fast and hot that the radiation from the shocked matter dominates the energy transport. This in turn leads to changes in the shock structure. Radiative shocks are challenging to simulate, as they include phenomena on a range of spatial and temporal scales and involve two types of nonlinear physics – hydrodynamics and radiation transport. Even so, the range of physics involved is narrow enough that one can seek to model all of it with sufficient fidelity to reproduce the data.

The CRASH project builds upon the basic physical system shown in Figure 1. Ten (0.35 μm wavelength) laser beams from the Omega laser¹ are incident on a 20- μm thick Be disk, at an irradiance of $\sim 7 \times 10^{14} \text{ W/cm}^2$ for 1 ns. This shocks the Be and then accelerates the resulting plasma to $> 150 \text{ km/s}$. The leading edge of this plasma drives a shock into Xe gas at 1.1 atm pressure with an initial velocity of $\sim 200 \text{ km/s}$. This produces the observable structures shown schematically in Figure 1b and by a radiograph in Figure 1c. The radiation from the shocked Xe preheats the unshocked Xe. It also ablates the shock-tube wall, producing a “wall shock” that drives the Xe gas inward. Where this wall shock meets the primary shock, the shock-shock interaction produces a measurable deflection of the dense Xe flow (dark in the radiograph). The Xe that flows through both the wall shock and the oblique portion of the primary shock ends up with higher velocity and forms the material described as entrained Xe. On a finer scale than is seen in the radiograph, the shocked Xe ions, which are initially heated to hundreds of eV, cool rapidly as they heat the electrons and are further ionized, and the heated electrons radiate most of their energy away. In response, the shocked Xe layer, which is optically very thick, becomes several times denser. The resulting final temperature in the shocked matter and characteristic radiation temperature is about 40 eV. In contrast, the radiation mean free path in

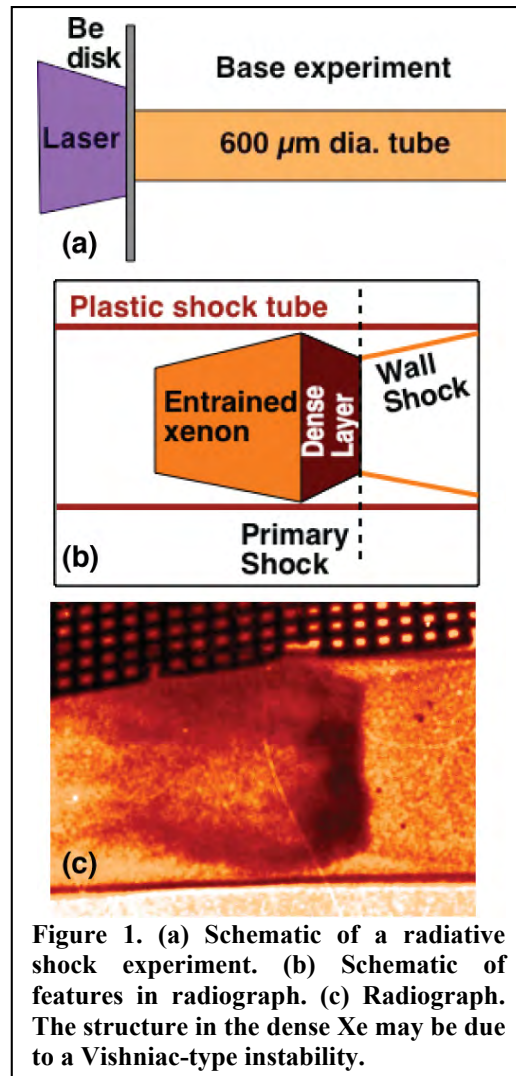
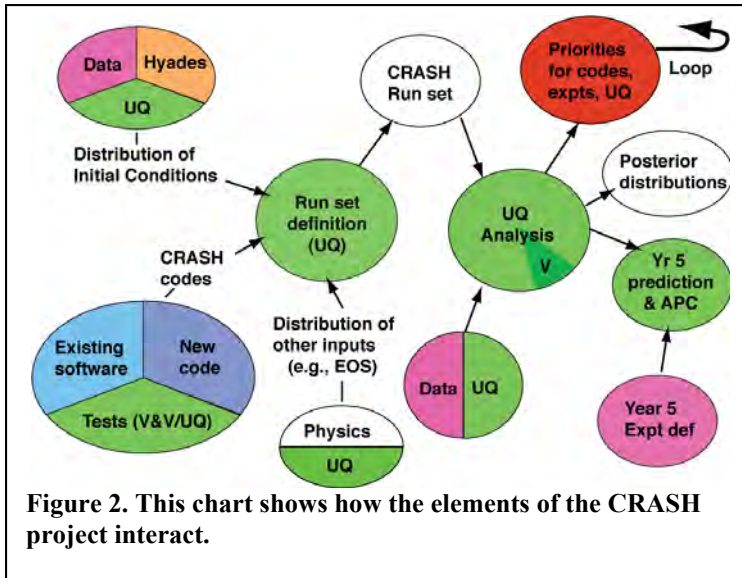


Figure 1. (a) Schematic of a radiative shock experiment. (b) Schematic of features in radiograph. (c) Radiograph. The structure in the dense Xe may be due to a Vishniac-type instability.



the unshocked Xe is much longer and the radiation transport is not diffusive.

The project goal described above has implications for the execution of the project, illustrated in Figure. 2. During this past year we have covered most of this plot for the first time. The green colors illustrate those places in the project where uncertainty quantification enters into the project activity. We will use this

figure to illustrate and discuss the project elements. Just to the left of the center of the figure is a bubble labeled “Run set definition”. The task of this activity, which involves both statistical analysis and physical evidence, is to define a set of computer simulation runs that cover in a sensible way the space of uncertainty associated with the physical system of interest and our models of it. We will return to this task after discussing the three bubbles that feed into it.

The bubble at the upper left describes the physical information that is necessary to characterize the initial physical conditions for the simulation runs. The first element of this is data from and about the physical experiments. This includes both measured results and experimental uncertainties, such as the actual thickness of the Be disk. In the past year we used the results of experiments in October 2008 regarding shock position at 13 ns as input to our first predictive capability study, which used 1D simulations. In December 2009 we obtained data regarding the shock penetration through the Be disk, which will become the primary evidence used in calibrating the physical conditions used as input to the CRASH code.

Because the CRASH code does not model laser energy deposition, simulation runs using the Lagrangian, radiation-hydrodynamics code HYADES, in combination with physical data, are used to produce the initial conditions for CRASH. Our 1D study, described in more detail below, involved several hundred HYADES runs used to determine conditions at 1.3 ns into the experiment. There were multiple elements of uncertainty quantification associated with this process. This set of runs was designed using statistical methods to span the 15 variables judged to be of greatest potential importance. The variables reflected analysis of the experimental inputs and data and analysis of the variables that were inputs to the code. We analyzed the results of these runs to extract features from them and produce a “Physics Informed Emulator”, in which we statistically described the profiles of the physical variables and their variations at 1.3 ns. We used this emulator to define the input space for the CRASH run set.

A final element of the upper left bubble has been the completion of a set of 2D HYADES runs, also described below, for our next predictive capability study. Also, further evaluation of the experimental uncertainties showed that the laser pulse never extends beyond 1.1 ns, which has become our new initiation time for the CRASH simulations. We developed automatic rezoning methods for 2D HYADES that have reduced the manpower required to complete one of these runs by at least an order of magnitude. This new, statistically designed run set covered five variables in 104 runs. (The 1D analysis showed that most of the 15 variables used were not significant.) Unfortunately, the automatic rezoning also affects the results, in ways we discuss further below.

The lower left bubble in Figure 2 designates the development, testing, and characterization of the CRASH simulation code. This has included the addition of features to the previously existing BATSRUS code. The CRASH 1.0 release of a year ago included a gray-diffusion radiation model, a level-set method for interface tracking, and other features needed to model this high-energy-density system. The CRASH 2.0 beta includes multigroup diffusion, electron physics and electron heat conduction, and dynamic adaptive mesh refinement. These features are discussed at length below. CRASH 2.0 contains the minimum set of features we believe should be necessary for reasonably accurate modeling of the experiment. The PDT code, which implements a higher fidelity radiation transport method, is now ready for integration with BATSRUS. However, a member of our TST raised the issue of whether the integrated code would be considered UCNI. While we pursue this question, we have decided to first address the question of how essential to simulations of our physical system is the fidelity that PDT makes possible. Both BATSRUS and PDT have very extensive suites of verification tests, run on multiple platforms on a regular basis. These are described in more detail below. In the next year we will supplement these with additional verification tests, validation studies, and quantitative assessments of numerical uncertainties.

The final bubble that provides input to a CRASH run set is labeled “Physics.” This designates the evaluation of physical parameters that are needed by the code, notably equations of state (EOS), opacities, and physical coefficients. The CRASH code can accommodate tabular input for EOS and opacities. Our baseline method is to generate these from a self-consistent model based on first principles. The reasons for this and the results to date are discussed below.

Returning then to the “Run set definition” bubble, a CRASH run set is statistically defined to cover (in principle) variations in the initial conditions, in the physical parameters, in features that determine numerical accuracy, and in model fidelity. In practice, sensitivity studies and perhaps other methods are used to select those variables having the most significant impact on the results of interest. The run set definition leads to a CRASH run set. We have done a number of run sets, using 1D or 3D CRASH, discussed below.

The bubble labeled “UQ analysis” covers a range of activities that utilize the output of CRASH run sets, indicated schematically by other features on the chart. The other input to these activities is experimental data and independent analysis of its uncertainties, as

illustrated. At present, these data are extracted from the radiographs obtained in October 2008. The outputs of the CRASH run set are then post-processed to extract the same features that can be measured from the physical data, such as the shock position the shocked Xe layer thickness (between the primary shock and the Be), and the thickness and length of the entrained Xe annulus flowing through the wall shock, as seen in Figure 1. We then analyze these results in conjunction with the physical data to produce an assessment of the accuracy of the predictions and of model errors. Formally, these results provide posterior distributions of those input parameters considered as calibration parameters, and distributions of output parameters, as shown on the chart in Figure 2.

When this process is undertaken using the definition of a future experiment as the basis for the runs and analysis, which will happen for the first time in the next year, the result is a prediction and an assessment of predictive capability for that experiment. We will first apply this to a late-observation-time baseline experiment, to be performed in August 2010. We will next apply it to the year-3 experiment, which will be defined this coming summer, with input from our UQ process. It will then be applied to the year-5 experiment, which features a radiative shock driven through a nozzle and into an elliptical tube.

The UQ analysis of the run sets, combined with other knowledge of the physical system and the project, then forms the basis for decisions about priorities as the project moves forward. The upper right bubble illustrates this, and the fact that this leads us to loop back and take another pass through the process. Finally, another aspect of UQ analysis of run sets is to do verification of the UQ methods (shown as the “V” in the bubble). One such study, involving a shock-tube problem, is discussed below.

Two important aspects of the project are not captured fully by the chart in Figure 2. The first of these is physics. Both annual review reports have emphasized the importance of advancing our understanding and documentation of the physics of the CRASH system. To this end we have produced a “CRASH basics” document used by the team to understand the basic behavior of the system and many of the physical parameters of interest. More recently, we have produced an analytic analysis of x-ray-driven walls, like those that generate the wall shock. This showed that the generation of the wall shock is quite sensitive to the x-ray radiation input. We are working to compare the results with both CRASH and Hyades calculations. We also have produced documentation describing in detail our EOS and opacity calculations. In addition, we have published or submitted several papers further describing the properties and behavior of the CRASH system,²⁻⁷ and have others in preparation.

The second, additional important aspect of the project is education and training. Training of graduate students is an important aspect of CRASH. At present, we have 21 graduate students whose research is or will be supported at least in part by the Center. Their research activities, and those of our three recent graduates, are described in a section below. These students are working on all aspects of the project, including experiments, fluid dynamics modeling, radiation transport methods, and APC methods. In addition, several of these students, and several from outside the CRASH project, are enrolled in the

Scientific Computing certificate program. This program requires several courses in numerical methods, several courses in computer science, in addition to the requirements for the PhD in the student's home department. Some of the CRASH students enrolled in the certificate program are pursuing the Predictive Science track of the Scientific Computing certificate. At both UM and TAMU, courses in uncertainty quantification and sensitivity analysis were introduced this year, for CRASH students and other students interested in learning about UQ. The course at TAMU, first offered in Fall 2009 and taught by Ryan McClarren, focused on verification, validation, sensitivity analysis and UQ. The course at UM, first offered in Winter 2010 and taught by James Holloway, Vijay Nair and Ken Powell, focused on input/output modeling, screening and sensitivity analysis, and UQ. Both courses included homework covering basic topics, and culminated with student independent projects. More than two dozen students took these courses.

II. Assessment of Predictive Capability (APC)

Our overarching project goal is to develop a simulator – the CRASH code – that can predict radiative shock behavior in an unexplored region of the experimental input space – the elliptical tube – after being assessed in a different region of input space that has been explored by experiments. Our unique intended contribution is to be the first academic team to use statistical assessment of predictive capability to systematically guide improvements in simulations and improvement in experiments so as to produce new predictions of improved accuracy, and to demonstrate this improvement by experiment. CRASH employs both sensitivity studies, to assess which aspects of the physical system are important and which are not, and predictive model construction, to assess the probability distribution functions of both physical parameters and experimental outputs. The present section provides an overview, describes our first end-to-end predictive study, and reports some related work.

A. Overview of CRASH UQ methodology

Predictive science is more than prediction. Predictive science is the use of physics modeling, often realized in complex computer codes, to forecast what would be observed in reality should a field experiment be conducted in reality. Such a forecast should include:

- estimates of the sensitivity of the output y to variations in the input (x, θ)
- an understanding of the significant sources of uncertainty that effect the output
- the construction of a predictive distribution of outputs y .

Here x and θ designate experimental parameters and physical constants, respectively. These are discussed further below. Successful prediction means that the field experimental result is, with reasonable probability, within the range predicted by the code. Successful prediction can be hampered by inadequate physics modeling, ignorance of physical constants, lack of numerical convergence or robustness, or inherent natural limits due to sensitivity (as arises, for example, in chaotic phenomena). Within the

context of our uncertainty quantification, *predictive modeling* means computing an estimate of the probability distribution function (pdf) of the outputs generated by the pdf of the inputs for a prospective field experiment, informed by both simulation and prior field experiments. At the least, we would want an:

- estimate of the mean output (over the input uncertainties)
- estimate of the variance (or other uncertainty measure) of that mean.

But in general we want an estimate of the pdf of the simulation output that accounts for

- uncertainties in physics parameters θ
- uncertainties in experimental/design inputs x
- errors due to numerical methods
- uncertainties due to predictive model construction (statistical fitting)
- uncertainties in the physics modeling

all informed by comparison to a set of prior field (calibration) experiments.

In prediction and code improvements, there are two programs of research available:

- Using the combination of the code and field experiment data, we can produce a combined predictive model that is a better predictor than is either alone, but realistically this program only allows us to predict in areas of input space in which we have code runs and data. This is in some sense interpolation based on code and field experiments.
- Using the combination of code and field experiment data as well as expert judgment, to systematically indicate areas in need of modeling improvement, and to use the improved code to make predictions in new regimes of input space in which we may not have experimental results from the field. This is true prediction: extrapolation to a new region in which we can simulate, but have not yet collected field observations.

The second program, which is generally aligned with the CRASH project requirements, needs techniques that can allow us to systematically quantify the extent to which our code is predictive in areas of input space that we have measured with field experiments, and inference tools that can tell us where best to perform a next simulation run or a next field experiment. The complete prediction of uncertainty requires us to combine multiple input sets around any nominal field experiment, with input values drawn from best estimates of the pdfs for those inputs. This allows a mapping to the pdf from the inputs to the outputs, thereby providing information on uncertainty of the predictions.

Figure 3 illustrates our system of codes and related parameters. Our tools for studying our system consist of a code system, which is initialized with data Y_{HP} . The output of this code system, Y_C , is post processed into data Y_S that can be directly compared with experimental diagnostic outputs, Y_E . Each experiment corresponds to a physical setup x , which includes data about geometry, materials present, the time at which data are taken, etc. There are however, other data that must go into the simulation, including physics parameters (such as energy levels in our opacity and EOS models, or γ in a gamma law

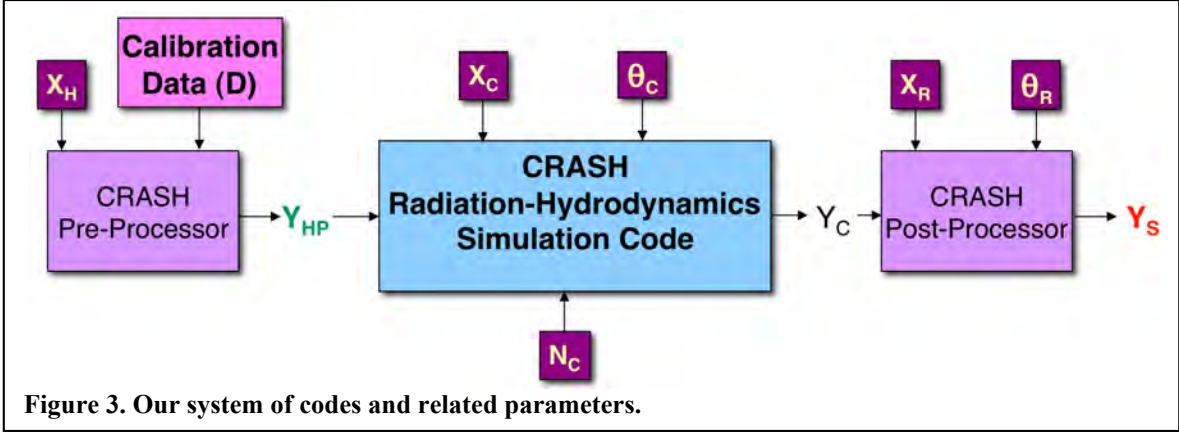


Figure 3. Our system of codes and related parameters.

EOS, or the opacity itself, depending on where we elect to study the uncertainty source). These data are generically called θ .

Generally our model cannot be evaluated exactly. It requires numerical integration of partial differential equations, or solutions of linear equations, and so forth, which cannot be exactly accomplished. Therefore, in practice we evaluate a function in which numeric parameters N represent parameters introduced in the approximate evaluation of the model. Examples of these are mesh sizes in a numerical computation, or a convergence criterion for a linear solver. Therefore, in the end we have

$$Y_s = \eta(x, \theta, Y_{HP}, N)$$

It should be noted here that the output Y_s may be very low dimensional; these are just the few parameters that we measure, not the full field that describes the continuum physics. The input, by contrast, might be rather high dimensional, as Y_{HP} must define the initial state of the system. Our code system is designed to minimize tuning parameters. While the system η does depend on numerical parameters N , our strategy regarding these is to confirm that the mesh is sufficiently resolved, for example, so that the uncertainty generated in the output Y_s by N is smaller than the experimental uncertainty. These latter two points are worthy of note: a goal of CRASH is, to the largest extent possible, to make predictions with minimal tuning and without treating numerical choices as either physics or tuning. Our program of extrapolation requires that any tuning is accomplished using data corresponding to a region of input space where we run initial field experiments, and then use the posterior pdfs for those θ in another region of space to make the year 5 prediction.

B. Predictive capability study using 1D simulations

In order to gain experience with the complete process of doing a predictive capability study, we undertook a study based on one-dimensional computations during this past year. Here we discuss this study and its results in several phases.

a. 1D HYADES sensitivity study

Because CRASH is being initialized based on output from runs using two-dimensional HYADES (H2D), in order to have a calibrated initial condition modeling the laser irradiation phase of the experiment, it is important to assess the uncertainties associated with H2D to gain a full understanding of the uncertainties in CRASH. Lagrangian simulations in 2D can be very time and effort intensive due to mesh-tangling issues, which is one of several reasons why the first uncertainty study was done using 1D HYADES. The results of this study provided evidence of the importance of different parameters within the 1D code and were used to direct the future 2D study. A 15-D parameter space-filling Latin hypercube distribution was designed by Derek Bingham at Simon Fraser University to define a 512-run dataset for HYADES. The 15 parameters are as follows:

- Drive Laser Energy
- Drive Disk Thickness
- Gas Density
- Drive Pulse Duration
- Tube Length
- Laser Rise Time
- Slope of Laser Pulse
- Mesh Resolution
- Photon Group Resolution
- Electron Flux Limiter
- Time Step Multiplier
- Beryllium Opacity scale factor
- Beryllium Gamma
- Xenon Gamma
- Xenon Opacity scale factor

The parameter list encompasses both experimental parameters, such as the laser energy and the gas density, as well as physical or numerical code parameters, such as the xenon gamma or the mesh resolution. The experimental parameters were varied over a range defined by estimates of the variances from the experiments carried out at the Omega laser facility. The ranges of the code parameters were determined by careful analysis of sensible ranges for each variable. The results from the 1D uncertainty study were then used to further refine what we consider to be a sensible range of parameters for the H2D simulations. Before undertaking the full study, test runs were done to confirm the exclusion of some other parameters on the grounds that we did not believe they could have significant effects.

Experimental conditions - the pressure, location, velocity and density - from ten locations in the 1D output from the HYADES runs at 1.3 ns were collected into a large dataset used for sensitivity analysis and uncertainty quantification. The choice for the ten locations was motivated by what features would be important to develop a physics-informed emulator for the 1D code. The locations were:

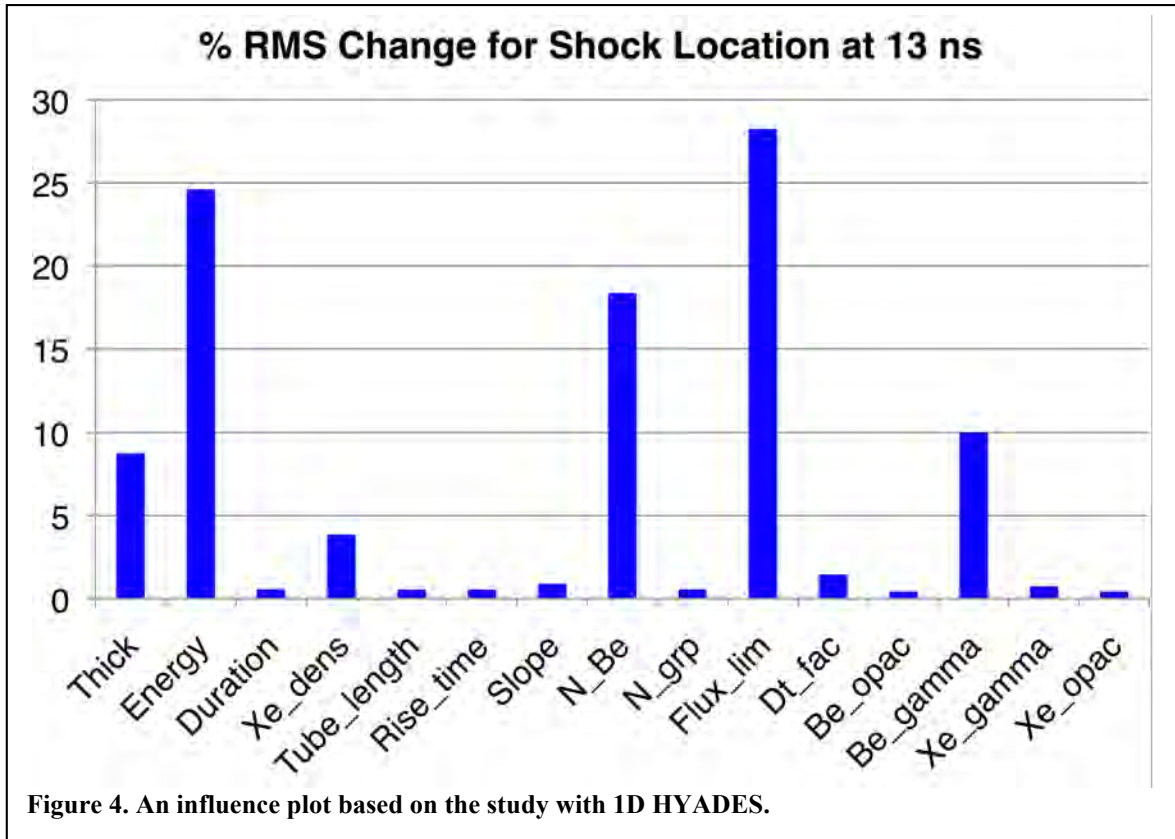
- Where the velocity first exceeds -3×10^7 cm/s, in order to fit to the ablating material
- Where the density is 1/2 the maximum density, in order to fit an intermediate point in the density profile
- First two abrupt decreases in the derivative of the pressure, in order to fit well the pressure profile in the beryllium
- Where the beryllium reached its maximum density
- Where the beryllium reached its maximum velocity
- The locations of the zone of beryllium and the zone of xenon adjacent to the interface
- The shock location in the xenon, in order to fit the shocked material
- A location 500 microns ahead of the shock where the precursor properties are steady in order to fit to the remainder of the material

These ten locations were used to design the physics-informed emulator for 1D HYADES as well as to assess the sensitivities and uncertainties in HYADES related to different input parameters. The location of the shock at 13 ns was also extracted from the 1D HYADES results and used for sensitivity analysis. A power-law curve was fit to the shock locations from 1.5 ns to 16 ns in increments of .25 ns and used to extract the position of the shock at 13 ns. This was done in order to remove the discretization error associated with picking the shock to be located in a particular zone and choosing that zone's location as the shock location.

b. Sensitivity studies

We evaluated global sensitivity by functional fitting with flexible regression methods (e.g. MARS and MART) followed by random permutations of each input and computation of average RMS change over such permutations. Using this technique we are able to determine which inputs have the most significant effect on the response surface. These results are plotted in *influence plots* to show those inputs that have the largest global influence on the outputs. Figure 4 shows an influence plot based on using 1D HYADES.

This identifies the Be disk thickness, gamma (the ratio of specific heats), and laser energy as important physical variables to the output, over the ranges investigated. Also notable is the number of zones (N_{Be}) used in the code; this set of data is based on a 512 point input design over a 15 dimensional input space. In using this set of data to construct the initial state for CRASH, we marginalize over only those values of N_{Be} that have no influence on the outputs (that is, we use sufficiently large N_{Be} that this mesh parameter has no influence on the results). The heat conduction flux limiter also stands tall as having a large influence. This then tells us that we should more closely investigate this parameter; subsequent review of the literature indicates that we should have used a more restricted range of values for the heat conduction flux limiter. In this way the sensitivity study makes apparent parameters that require more attention, and the UQ process drives the physics modeling and code development.



Another sensitivity metric comes from the length parameters from Gaussian Process (GP) fits of response surfaces. The covariance models in the GP model have the form

$$\prod_{k=1}^K \exp\left[-\frac{(x_k^{\text{ref}} - x_k)^2}{2l_k^2}\right],$$

where l_k is the length parameter along coordinate k . A large length scale implies that distant points are highly correlated. The “relative relevance” for input k is defined as $r_k = 1/l_k$; a small value for r_k means that large changes in variable x_k have little relevance to the output, while large values of r_k imply that a small change in x_k has a significant relevance to the output. While the influence plots describe large-scale influences of inputs on outputs, they operate over the whole input range and are not sensitive to more local structure. The relative relevance describes the scale over which a variable operates, and so provides information about variations that are more localized than the entire input range investigated.

Figure 5 shows the relative relevance of the 15 input parameters for shock location at 1.3 ns (at the time when CRASH was initialized). The input variables have been standardized over their ranges, so the relative relevance is normalized to the width of the input space along each dimension. In the system response at this early time more input variables are in play, besides those that have influence at 13 ns. In particular, besides the influential 5 variables seen before, pulse duration and number of groups (N_grp), all produce

relatively rapid variation in output compared to the other 8 variables. These then become candidates for closer study. A study of the variation in N_{Be} marginalized over all other variables reveals a curve asymptoting to a shock location independent of N_{Be} (number of Be zones), as would be expected.

c. Predictive model construction

We often need to create *predictive models* of outputs (such as shock position or shocked Xe layer thickness). We do this by combining the CRASH field experiment data and CRASH code runs, along with prior distributions of physics parameters $\pi(\theta)$. The predictive model, based generally on the ideas of Kennedy and O'Hagan, will be of the form

$$Y = \eta(x, \theta) + \delta(x) + \varepsilon,$$

where δ is the model discrepancy, and ε represents the measurement error, which in fact depend on the measured data and corresponding experimental inputs.

In the standard approach to this predictive model form the entire right hand side is described by hyper-parameters from a statistical fitting, and these are determined by a Bayesian formulation of the problem with a specified likelihood model. Gaussian processes models are used for the form of this fit. This process computes a posterior distribution for physics constants $\pi(\theta | Y_E, X_E)$ that can tighten our knowledge of those parameters given field measurements, and a predictive distribution $\pi(y | x, Y_E, X_E)$ for the output y of a new experiment x , again conditional on the field measurements.

Within the CRASH project we are interested in how we can use the discrepancy δ to help us identify defects in the modeling. Essentially, a larger δ suggests that there is more physics inadequacy. Changes to the physics modeling that decrease δ are generally speaking good changes, and δ therefore provides a metric against which to judge improvements in physics and numerics. Using δ in this way requires us to reconsider the common practice of jointly determining δ and calibrating the θ 's. A poor choice of θ can be balanced against a large discrepancy. We will therefore explore doing the calibration step of finding $\pi(\theta | Y_E, X_E)$ sequentially, before computing the discrepancy and $\pi(y | x, Y_E, X_E)$.

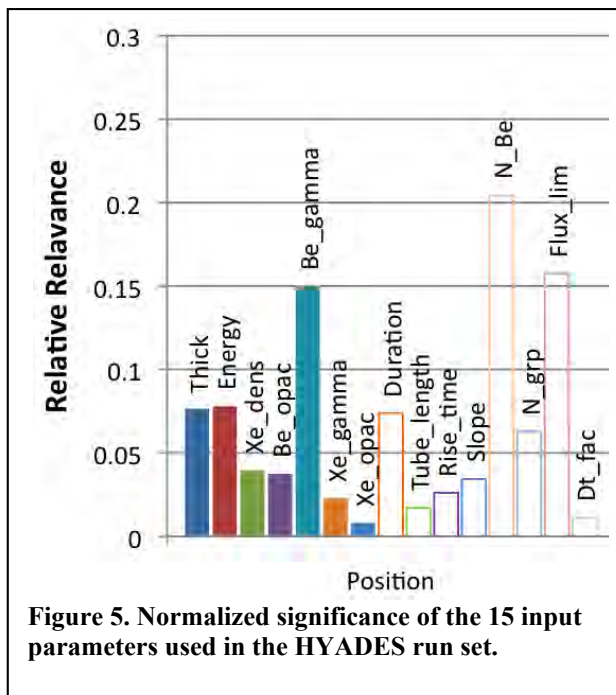


Figure 5. Normalized significance of the 15 input parameters used in the HYADES run set.

Table 1: Experimental parameters for first study

Description	Average/Typical Values
Be drive disk thickness	21 μm
Laser total energy	3870 J
Xe gas pressure	1.15 atm
Observation time t_o	13, 14 and 16 ns

Table 2: Physics parameters and their ranges.

Parameter	Nominal value	Range used
γ_{Be} Be gamma	5/3	1.4 to 5/3
γ_{Xe} Xe gamma	1.2	1.1 to 1.4
Be opacity Scale factor	1	0.7 to 1.3
Xe opacity Scale factor	1	0.7 to 1.3

A first predictive model has been constructed that combines the Omega field experiment campaign data from October 2008 with CRASH 1D runs. As part of this activity a model discrepancy function was created to provide a quantitative picture of the quality of the 1D CRASH model compared to experiments; the goal of year 3 will be to reduce this discrepancy using the improved physics of 2D CRASH 2.0. Further goals of the task are therefore to explore the best ways to create this discrepancy function, and to learn what

changes in the CRASH code physics will reduce it. Finally, we will predict results from one Omega experiment and compare it to the actual data.

While the discrepancy gives us a tool on which to base decisions, we cannot pursue its reduction slavishly. In the long run we want to use it to improve physics so that we can improve confidence in CRASH to predict an experiment we have not conducted and which is in a somewhat different region of input space (oval vs. circular tube), rather than to optimize CRASH to reproduce the experiments we already have. Table 1 shows the inputs x for this model and Table 2 shows the physics parameters θ .

Table 3. Actual experimental values.

Shot number	Be Thickness (μm)	Laser Energy (J)	Xe Pressure (atm)	t_o (ns)
52661	21	3889.6	1.133	14
52661*	21	3889.6	1.133	16
52663	21	3882	1.167	13
52665	21	3892.4	1.133	13
52665*	21	3892.4	1.133	14
52667	21	3880.2	1.204	13
52667*	21	3880.2	1.204	13
52668	21	3859.8	1.105	13
52668*	21	3859.8	1.105	14
52669	21	3846	1.169	13
52670	21	3841.5	1.17	14
52671	21	3867.4	1.169	13

Note that the observation times, t_o , of the Omega data are at 13 ns, 14 ns, or 16 ns. We treat this as an input to CRASH because our measured data are at different values of t_o . The physics parameters are in some sense “a step backwards” for this first CRASH UQ exercise. While CRASH has a sophisticated equation of state, in this first exercise we used constant γ -law equation of state for Xe and Be, and introduced opacity scale factors on the nominal opacity from SESAME tables. In total, then, we have an 8-dimensional input space from the UQ perspective.

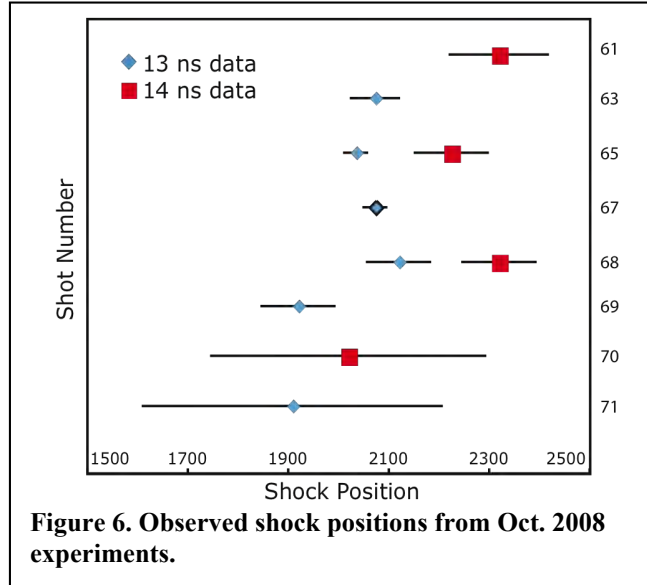


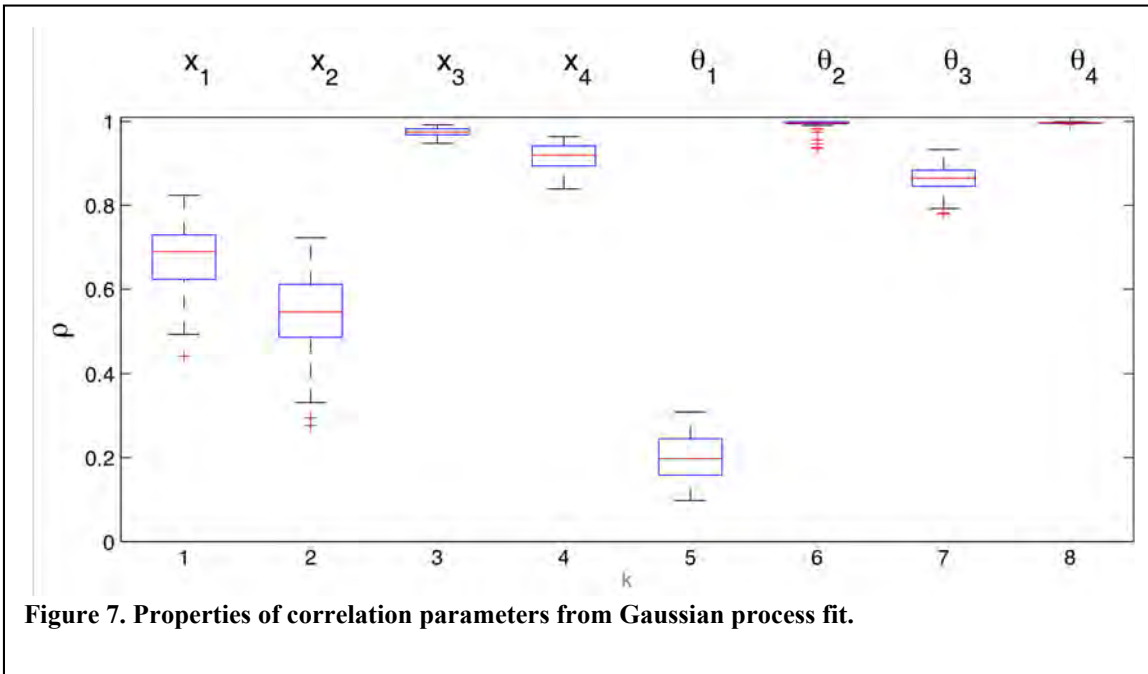
Figure 6. Observed shock positions from Oct. 2008 experiments.

In October 2008 we conducted a set of shots on Omega designed primarily to explore the variability of the experimental data. These were used as our first set of data to build a calibrated predictive model. The shot numbers and input data are shown in Table 3. Table 3 shows the Omega shot numbers and experimentally controlled variables. Note that two views are available for some shots, yielding two observation times for some shots, and one repeated observation time (the two views were taken simultaneously). From our perspective, these 8 shots yield 12 measurements of the outputs y . Data from the second view are marked with asterisks (*)

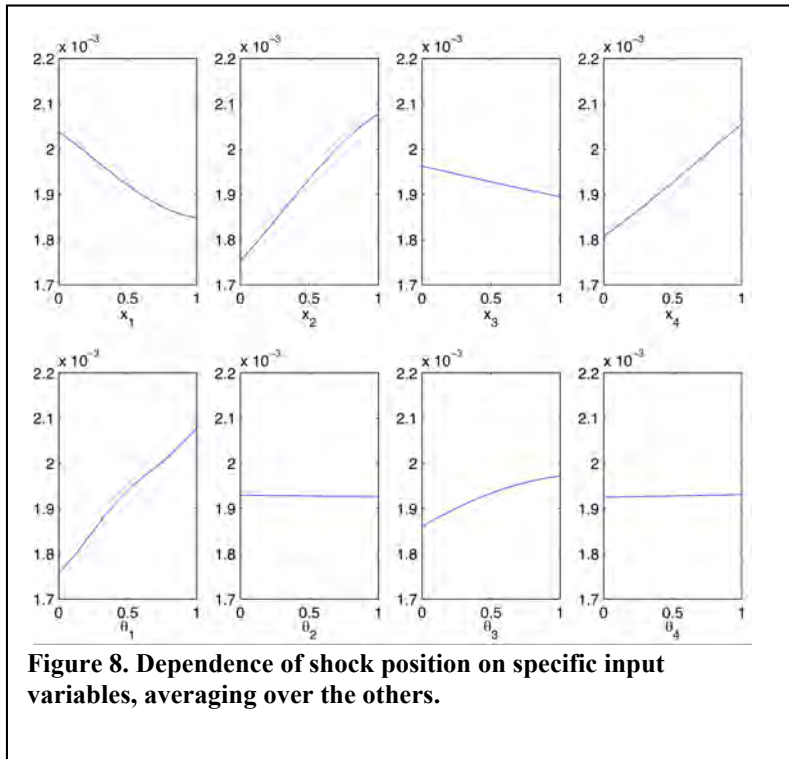
Figure 6 shows the shock location data from the October shots. View 2 in shot 52661 is at 16 ns, and is not shown on this plot. For this UQ exercise we used 9 experimental points (8 as prior experiments, and the 9th to predict); we eliminated the data marked 52661* because it is at a late time, and 52670 & 52671 because these had alignment issues that led to a shock what was not perpendicular to the tube.

To construct the joint fitting of the output y from both experiment and simulation, the input space must be sampled for the simulator runs. The input design for the simulator consists of two parts: 1) A 256-point design over 8 input parameters (4 x 's and 4 θ 's), and 2) a 64-point design over the input space that should match the 8 experimental x values, and for each of these provides 8 θ 's to sample the calibration space around the experimental observations. The 256-point design is an orthogonal array-based Latin hypercube with a space-filling criterion added to spread out the points. The 64-point part of the design allows the code to simulate at the nominal experimental input values, and so produce well quantified values of the discrepancy at those points.

The correlation parameters from the Gaussian process fit again provide a measure of sensitivity, as shown in Figure 7. These identify Be thickness, laser energy, and observation time as the most sensitive input parameters x , and Be gamma and Be opacity as the most important θ 's. The box and whisker plots in this figure show the median (red)



as well as the first and second quartiles. The whiskers are at the last data point that is within 1.5 of the interquartile range. Red crosses are outliers. Figure 8 shows single effects plots of the shock location as functions of each of the inputs in turn, in each case averaged over the other 7 input dimensions. The input ranges are scaled to the range [0,1] in each case. A study of these along with a knowledge of the expected range of experimental input values and



knowledge of the posterior pdfs for the calibration variables allows us to produce an uncertainty budget, as shown in Table 4. This budget shows 6 sources of uncertainty, and the approximate uncertainty in source location due to each of these sources, compared to the experimental measurement uncertainty. The first 3, Be gamma, PIE, and discrepancy are all related to modeling, while the other 3, Be disk thickness, Xe fill pressure, and laser energy, are experimental inputs.

Source	Uncertainty in Shock Location
Be Gamma	~ 0.15 mm
Physics Informed Emulator	~ 0.10 mm
Discrepancy	~ 0.07 mm
Be Disk Thickness	~ 0.10 mm
Xe Fill Pressure	~ 0.04 mm
Laser Energy	~ 0.01 mm
Experimental Uncertainties	~ 0.10 mm

To evaluate predictive ability we hold one experiment out, use only the 8 remaining field experiments to construct the model, and predict the ninth. This is repeated for each experiment. As an example of the model output, Figure 9 shows the posterior distribution of the location of a single shock

The results for the 9 “leave one out” fits are shown in Figure 10, along with 95% confidence intervals on the

predictions. The experimental uncertainty in the shock location (not shown) is on the order of ± 0.05 mm. The figure labels each of the experiments being predicted, and also shows which experiments are at an observation of 13 ns and which are at 14 ns.

The experimental results are all well within the 90% confidence intervals of the predictions. For the two exceptions, shot 52669 and shot 52668, the experimental uncertainty is shown as a horizontal dotted line. This uncertainty accounted for, the 90% prediction interval is seen to be consistent with the experimental value. It should be noted that the set of measurements nominally corresponding to 13 ns show a considerable spread of observed shock locations. This spread could not initially be predicted by the uncertainty in the inputs. This caused us to explore the actually experimental uncertainty in the observation time. It was discovered that the experimental observation times are in fact ± 500 ps, and this is consistent with the spread in observations. This is an example of using the predictive model to identify a area in which further understanding was needed. In fact much was learned about the absolute and relative timing uncertainties of the experimental facilities because of our investigation of this data.

We also used the predictive model to extrapolate to an observation time of 16 ns. The predicted shock location is 2.38 mm, while the experimental observation for

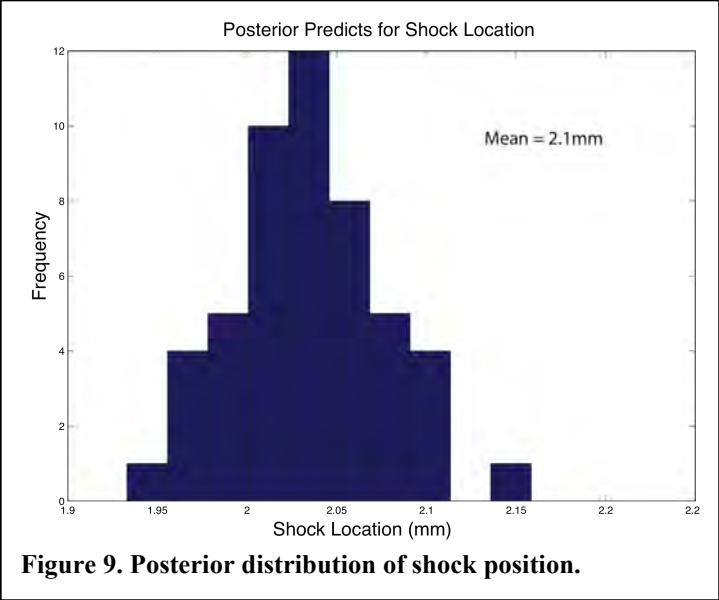


Figure 9. Posterior distribution of shock position.

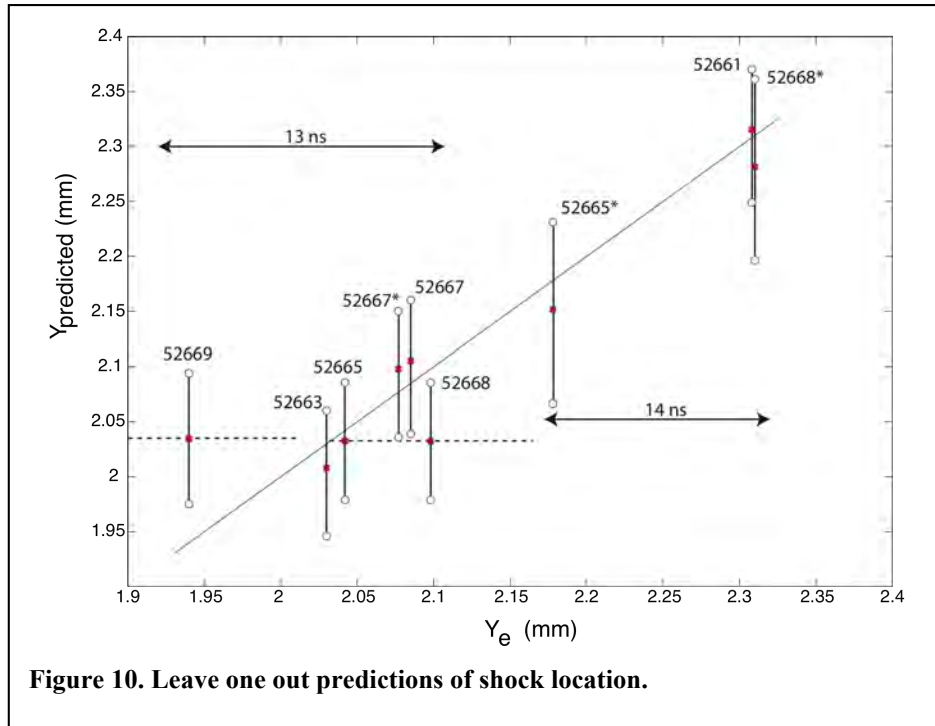


Figure 10. Leave one out predictions of shock location.

16 ns is 2.48 mm. The difference of 0.1 mm (100 microns) is comparable to the experimental and the predictive uncertainty.

B. Sensitivity analysis from three-dimensional simulations

One-dimensional studies can provide useful information about the sensitivities of output quantities of interest to variations in the input parameters. However, a number of important output features, such as the wall shock, cannot appear in one-dimensional geometry. As a result, we performed a preliminary three-dimensional sensitivity study of the baseline CRASH experiment. Each simulation was performed on a uniform Cartesian 1200 x 240 x 240 mesh using the CRASH code. A second set of runs was performed on a 600 x 120 x 120 mesh to test grid convergence. For this preliminary analysis, we used simplified physics, treating each material as a gamma-law gas and computed radiation transport with gray flux-limited diffusion. All simulations were initialized from a two-dimensional HYADES output file at 1.3 ns using nominal values of the input parameters. Each simulation required approximately 5 hours on 1024 cores of Hera at LLNL. The entire set of simulations was completed in about 2 weeks.

The study consisted of 64 simulations at each grid resolution varying four input parameters: the equation of state gamma for Be was varied between 1.4 and 1.66667; the gamma for Xe was varied between 1.1 and 1.4; and the opacity scale factors for both Be and Xe were varied independently between 0.7 and 1.3. The parameter combinations were determined using a Latin hypercube design. All other parameters were fixed at their nominal values. We examined three output quantities of interest – the location of the main shock, the angle between the wall shock and the plastic tube, and the distance of the triple point from the wall. A typical result showing these output quantities is plotted in

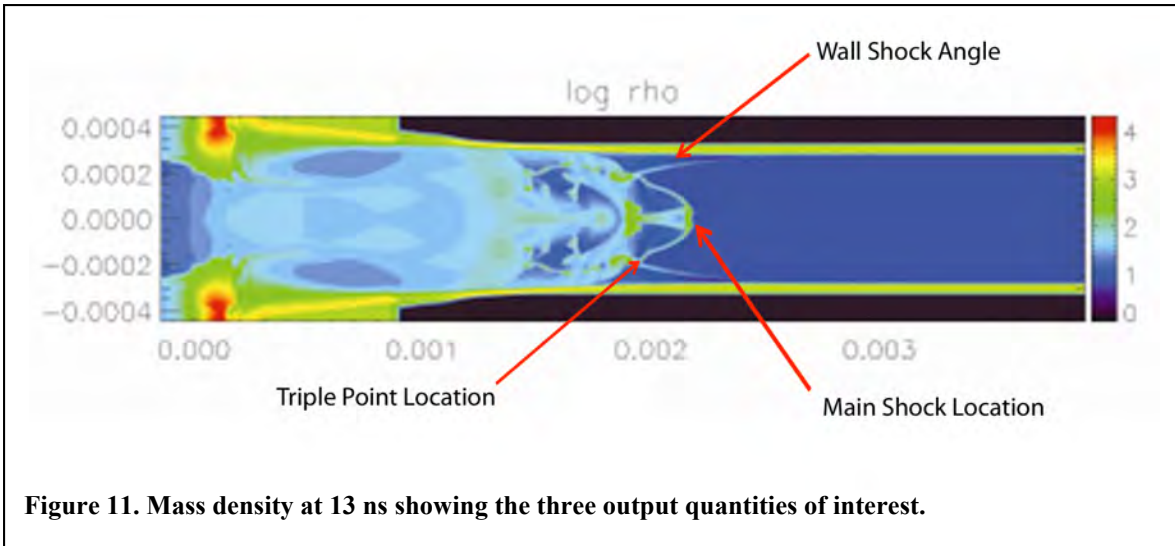


Figure 11. Mass density at 13 ns showing the three output quantities of interest.

Figure 11. All three of these quantities showed surprisingly good agreement with the experiments, even though the overall morphology of the flow in the experiments shows significant differences from the simulations. Figure 12 gives an indication of the wide variety of flow morphologies that are possible with different combinations of the input parameters.

The results indicate that the location of the main shock, defined here as the forward most location of a significant density jump in the xenon, is quite insensitive to the variations in these input parameters. The variation in location was much smaller than the range of values observed in the experiment. However, the shock location may still be sensitive to

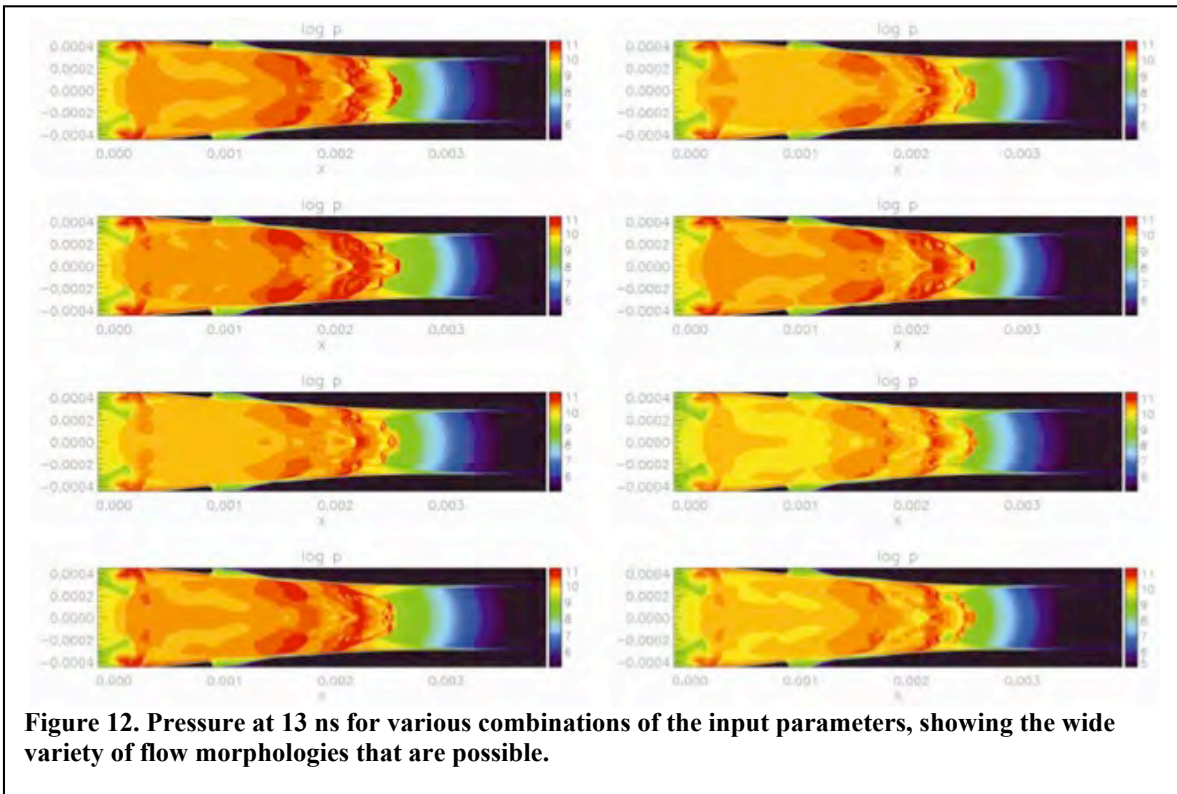


Figure 12. Pressure at 13 ns for various combinations of the input parameters, showing the wide variety of flow morphologies that are possible.

variations in these input parameters during the first 1.3 ns, before the initialization of the three-dimensional CRASH simulations. We also observed that the location of the main shock is not converged at these grid resolutions, although the error is still less than the experimental range. The angle of the wall shock shows a strong linear correlation with Xe opacity, but no correlation with the other three input variables. This makes physical sense, since the Xe opacity determines how far the radiation can penetrate ahead of the shock. For lower opacities, the wall shock begins further down the tube so that the angle is reduced. The triple point location shows a weak correlation with the Xe gamma, but no noticeable correlations with the other three input variables.

We also constructed plots showing relative importance of the input parameter variations using both MARS and MART. The two methods produced nearly identical results. The most important source of variation in the shock location is the Xe opacity scale factor, although as stated above, the variation in position is very small (at least after 1.3 ns). As expected, the variation in wall shock angle is determined entirely by the Xe opacity scale factor. On the other hand, the Xe gamma is almost entirely responsible for the variation in the triple point location. However, as mentioned above, input parameters that did not prove to be important in this study may still be important during the first 1.3 ns.

C. Verification of uncertainty quantification software

Verification and validation of simulation codes has been a major topic of research for many years. However, little attention has been devoted to verification of software used for uncertainty quantification analysis. As a first step in this process, we have performed a UQ analysis using a simplified problem with an analytic solution to determine if our UQ software is producing sensible results. The analytic solution in this case can be used as a substitute for experimental data and compared to the simulation results. As part of the verification process, we compared the results from four different UQ methodologies – Gaussian process, MARS, Bayesian MARS, and MART. We also tested the ability of the UQ software to distinguish between active and inert input parameters. Finally, we performed a blind calibration of an input parameter whose correct value was known.

Table 5. Sensitivity study using Bayesian MARS showing the probability of importance of each primary effect as well as the most important interactions for the four feature locations in the shock tube solution.

x_{shk}		x_{cd}		x_{tail}		x_{head}	
Effect	Prob.	Effect	Prob.	Effect	Prob.	Effect	Prob.
ρ	1.00	ρ	1.00	ρ	1.00	ρ	1.00
P	1.00	P	1.00	P	1.00	P	1.00
γ	1.00	γ	1.00	γ	1.00	γ	1.00
(ρ, P)	0.64	(ρ, P)	0.02	(ρ, P, γ)	0.03	(ρ, P)	0.04
(ρ, P, r_4)	0.05	r_5	0.02	(P, γ)	0.02	r_5	0.02
(ρ, P, γ)	0.02	r_4	0.02	(ρ, P)	0.02	r_3	0.02
(ρ, γ)	0.02	(ρ, P, γ)	0.01	r_4	0.01	(ρ, r_4)	0.01
(ρ, P, r_3)	0.01	(ρ, r_4)	0.01	r_5	0.01	r_2	0.01
(P, γ)	0.01	r_2	0.01	(γ, r_1, r_2)	0.01	(ρ, P, r_1)	0.01
(P, γ, r_1)	0.01	(P, r_1)	0.01	(ρ, P, r_2)	0.01	r_4	0.01

The problem we studied was a simple shock tube, which exercised only the hydrodynamics solver in the code. The initial conditions consisted of gas at high density and pressure separated from a second gas with a lower density and pressure by a membrane. Both gases were initially at rest. The size of the jumps in density and pressure across the membrane were chosen to match those encountered in the CRASH experiments. Three input parameters were varied – the pressure and density in the high-density gas and the value of gamma in the equation of state. The pressure and density in the low-density gas were held fixed. Five inert input parameters that had no effect on the solution were also varied. The study consisted of 62 parameter combinations using a Latin hypercube design. The same parameter combinations were used for both the simulations and the analytic solutions. Eight output quantities were examined. These included the locations of the shock front x_{shk} , the contact discontinuity x_{cd} , the head of the rarefaction x_{head} , and the tail of the rarefaction, x_{tail} . The other four quantities were the values of density ρ_{shk} , pressure P_{shk} , and velocity u_{shk} behind the shock front and the value of density ρ_{cd} between the contact discontinuity and rarefaction. These four quantities are constant both in space and in time.

The simulations and analytic solutions were virtually identical, except for a small bias in detecting the locations of discontinuities on the finite difference grid. The sensitivity analysis performed using all four methods produced consistent, but not identical, results. Since the four methods use different measures of relative importance of the input parameters, perfect agreement was not expected. In addition, all four methods successfully distinguished between the active and inert variables.

Tables 5 and 6 contain the results obtained using Bayesian Mars. The first three lines show the probability that each of the three active input parameters is important in producing variations in each of the eight output parameters. The remaining lines show the probability that various two-way and three-way interactions are important. Variables r_1 through r_5 are the inert input parameters. As expected, none of these parameters are

Table 6. Sensitivity study using Bayesian MARS showing the probability of importance of each primary effect as well as the most important interactions for the other four output parameters of interest.

ρ_{shk}		ρ_{cd}		P_{shk}		u_{shk}	
Effect	Prob.	Effect	Prob.	Effect	Prob.	Effect	Prob.
ρ	1.00	ρ	1.00	ρ	1.00	ρ	1.00
P	1.00	P	1.00	P	1.00	P	1.00
γ	1.00	γ	1.00	γ	1.00	γ	1.00
(P, γ)	0.59	(ρ, P)	1.00	(ρ, P)	1.00	r_4	0.01
(ρ, γ, r_5)	0.07	(ρ, γ)	1.00	(P, γ)	0.52	(ρ, P)	0.01
(P, γ, r_3)	0.06	(P, γ)	1.00	(ρ, γ)	0.04	r_1	0.01
(ρ, P)	0.04	(P, γ, r_4)	0.04	(P, γ, r_3)	0.02	r_5	0.01
(P, γ, r_5)	0.03	(ρ, r_1)	0.03	r_2	0.02	(ρ, r_4)	0.01
r_2	0.02	(ρ, r_3, r_4)	0.02	(P, γ, r_5)	0.02	(ρ, γ)	0.01
(ρ, γ)	0.02	(γ, r_4, r_5)	0.02	(ρ, r_3, r_5)	0.01	r_2	0.01

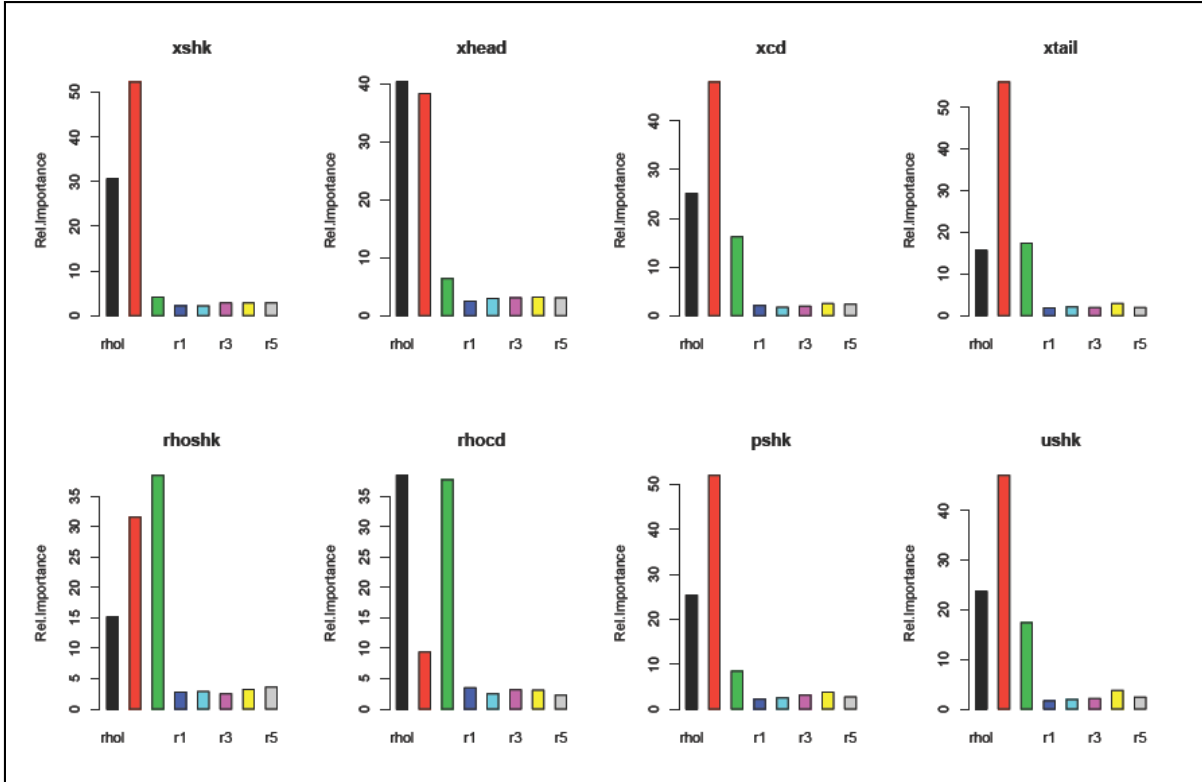


Figure 13. Relative importance plots obtained using MART. The first three columns are density, pressure, and gamma. The remaining five columns are inert parameters. Each plot shows results for one of the characteristic output variables.

important either by themselves or in interactions with other variables.

Figure 13 shows relative importance plots of the eight input variables for each of the output parameters. The first three columns represent the input density, pressure, and gamma followed by the five inert parameters. As expected, none of the five inert variables produced a significant signal in the analysis. The feature locations, shown in the top row of plots, are most sensitive to the initial density and pressure. However, the value of gamma is very important in determining the variability in the two density values.

The final test was to calibrate the value of gamma. A set of ten analytic solutions was computed varying only the density and pressure with gamma fixed at 1.4. The number of analytic solutions was reduced for this study to represent the normal case where there are many fewer experiments than simulations. These results were compared with the full set of numerical simulations in which all three input parameters were varied. The posterior distribution for gamma, shown in Figure 14, had a mean of 1.41, in excellent agreement with the expected value. As the number of analytic solutions is increased, the mean of the posterior distribution of gamma converges to the correct value and the standard deviation decreases.

In summary, all four of our UQ methods work well for this problem and provide believable results that are consistent with each other and with the physics of the problem. They reliably differentiated between active and inert input parameters and produced

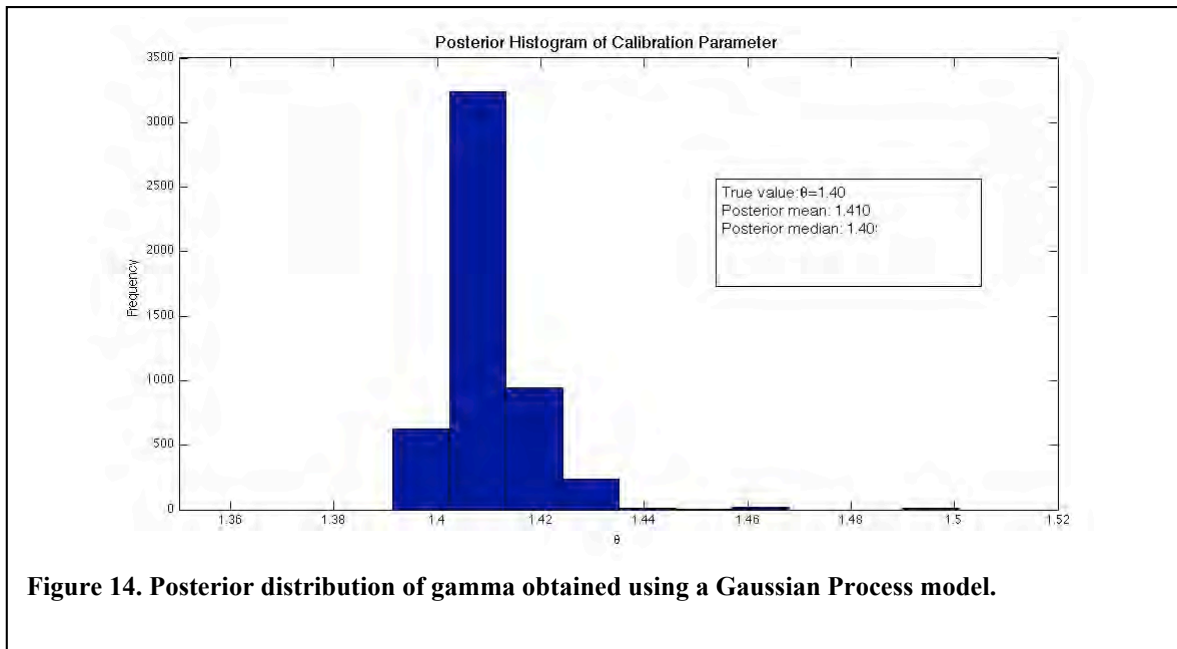


Figure 14. Posterior distribution of gamma obtained using a Gaussian Process model.

reasonable posterior distributions for calibrating the value of gamma. From this study, it appears that all four of our UQ methods should provide reliable results when applied to simulations and experiments of the complete CRASH problem.

D. 2D HYADES run set

Given the results from the 1D HYADES study, we have undertaken an investigation of the uncertainties and sensitivities in H2D for the purpose of understanding the way they will propagate into CRASH. Because H2D is a 2D Lagrangian hydrodynamics code, the time to run sets of simulations, mainly due to mesh tangling issues, is typically much longer. As such, in this first exploration using H2D, we have varied 5 critical input variables. The Be gamma, laser energy, electron flux limiter, and Be drive disk thickness were the four most important parameters from the initial 1D study and as such are also being used in the 2D study. The opacity of the plastic wall material was also determined to be an important variable as it plays a critical role in the development of the wall shock. This was not a variable that could be investigated in 1D. As it was unclear how difficult the runs would prove to be, the design used 64 runs for an initial exploration, with four additional sets of 10 runs each that could better sample the parameter space of interest. The full set of 104 runs is now complete. The left image in Figure 15 shows characteristic density profiles at 1.1 ns. Over most of the tube area, the calculated structures are quite planar.

The number of zones in the laser-irradiated material was also shown to be a critical parameter from the 1D study, but its variation was deemed impractical for the first attempt at the 2D study because of the mesh tangling problems that the extra zones would induce. The 1D study did show that the effect of the resolution was not as important as

the zone number grew. A series of simulations in 2D were carried out to look at how the zoning in the beryllium would affect the shock speed in the beryllium and the breakout time of the shock from the disk. This was done with all other materials removed so we were only looking at the disk, varying the zones in the axial direction from 20 to 100 zones in steps of 20 zones. The results showed little variation between using 20 and using 40 zones in the beryllium and no variation between runs from 40 up to 100 zones. All runs used 10 zones feathered in the first 2 microns and then $(N - 10)$ zones from 2 to 20 microns where N was the number of zones as stated. For the 2D sensitivity study, 40 zones were used in the beryllium.

The ranges of the variables that are being explored were refined from the initial 1D study. Analysis of the beam energies from the CRASH experimental campaign showed a variance in total beam energy of +/- 5 % instead of 15% as had been initially estimated. This was due to the fact that the beam energies have more variance in experiments where the energy is near the maximum energy per beam, which played a role in the initial estimation. The CRASH experiments used 380 J per beam instead of the maximum of 500 J per beam, which tightened the variance. The sensible range for the electron flux limiter was determined to be from .05 to .075 instead of from .03 to .10 after further reading recently published journal articles and consultation with collaborators. The high end of the range on the gamma for beryllium was widened from 1.667 to 1.75 in order to

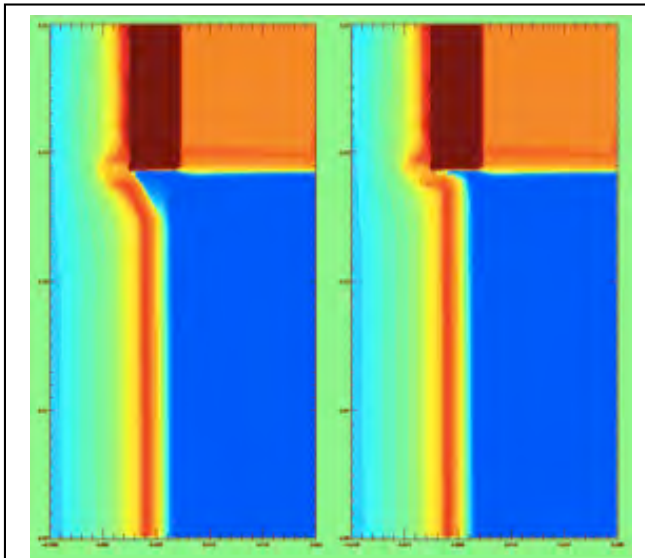


Figure 15. Mass density from 2D HYADES at 1.1 ns for the baseline CRASH experiment. The color scale displays mass density on an r-z plot, with a tube radius of 285 μm . The unshocked Xe is blue and the shocked Be is red. The image on the left, characteristic of the 104-run set, had the rezoner active in 6 zones in the Xe near the Be and the radial wall, vs 3 zones for the image on the right. This made an evident difference in the Be structure near the tube wall.

prevent the nominal value from being at the edge of the range. In addition, our previous estimate of the variation in the pulse duration turned out to be far larger than the reality. This allowed us to reduce the time when CRASH is initialized from 1.3 ns to 1.1 ns, and also implied that pulse variation was very clearly not a significant source of experimental variability.

The output will be extracted when the laser source ends, at 1.1 ns, for analysis. The breakout time of the shock from the beryllium is also to be extracted, as well as the time that the shock reaches both the 5-micron and 10-micron point in the beryllium disk. This data can be compared to the data from the CRASH Year 2 experiments.

In order for the simulations to reach the 1.1 ns point, H2D has implemented an auto-rezoning

capability. The auto-rezoner allows previously defined areas in the mesh to be rezoned following specified techniques at regular intervals. This allows the simulation to remap the mesh at locations where mesh tangling is a difficult issue, allowing the simulations to run longer without need for manual intervention. Mesh tangling problems still may happen in areas outside the rezoning regions, as well as in extreme cases in the rezoning regions. This necessitates the use of manual rezoning in order to untangle the mesh. Locations and times of tangling problems as well as the manual rezoning techniques used to fix them were documented for each of the runs in the set. A further analysis of the effects of the auto-rezoning on the simulation showed, unfortunately, that the profiles produced near the tube wall are quite sensitive to the rezoning details. Since the on-axis structures seen in the code results but not in the data from physical experiments appear to be generated from behavior at the tube walls early in time, this is a serious concern. The combination of this issue, of the delays involved in diagnosing and addressing issues with Hyades, and of the significant amount of manpower required to do H2D runs motivated us, as of the date of this report, to take a serious look at whether we should replace H2D with our own laser package.

E. Shock Morphology

If one compares the radiograph of Figure 1 with the density profiles of Figures 9 and 10 (or with the simulated radiographs of Figure 20 below), it is evident that the present calculation produces structure centered on the axis of the tube that is not present in the physical experiment. During the past several months, we have invested substantial effort in trying to understand this structure.

Specifically, the following numerical parameters were varied:

- Mesh resolution (including the addition of dynamic adaptive mesh refinement)
- Choice of numerical flux function
- Choice of limiter
- Symmetry of grid and initial conditions

While these affected the morphology of the entrained Xe layer, they did not affect the morphology of the primary shock.

The following changes to the fidelity of the physical model were made, again without changing the morphology of the primary shock:

- Multigroup flux-limited diffusion was added
- An electron physics package was added
- Extra materials present in the experiments (acrylic and gold) were added

We also examined EOS and opacity differences between HYADES and CRASH, and took several approaches to initialization of the CRASH runs, including initialization without using HYADES. Perhaps the most telling result is that shown in Figure 16, which is the result of a calculation entirely in CRASH using an x-ray source to launch a Be disk

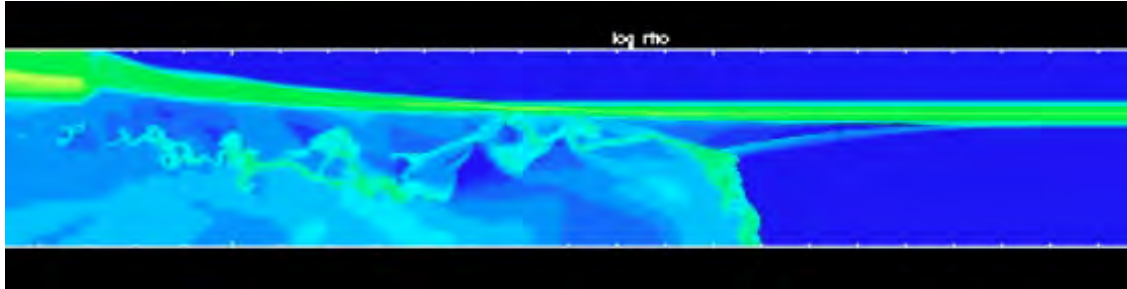


Figure 16. Log density plot at the observation time from an x-ray-driven radiative shock in CRASH.

that drives a radiative shock in Xe to the correct position at the observation time. The shock morphology in this case is qualitatively the same as that produced in the experiment. Interestingly, it is also possible to get a primary shock morphology similar to the HYADES/CRASH one in the x-ray-driven case, if the amount of energy deposited is higher than that shown in Figure 16.

Our conclusion from this work is that the structure we see in our baseline runs with HYADES-2D and CRASH is not a numerical effect, and is not a result from plausible errors in opacity or equation of state. It seems to be related to too much material coming off the wall, from one or both of the following:

- Too much energy deposited through the HYADES initial condition
- Over-prediction of wall heating by CRASH

The lack of adequate morphological similarity to data in our baseline simulations led us to decide to focus on issues of UQ methodology using 1D runs for our current set of predictive studies. We are continuing to explore potential causes of this issue while also considering whether to implement a laser package in CRASH.

III. Code development, verification, and testing

As the 2008 review team emphasized, this is where “the rubber meets the road” in the early phases of the CRASH project. Accordingly, it is the area of activity we initiated most quickly and focused on most strongly after the start of the project. In the first year we released CRASH 1.0, which contained the minimum capabilities to make a crude but physically somewhat reasonable approximation to the experiment. The past year has seen the implementation of those additional physics elements that we consider essential to the success of the CRASH project. Here we summarize the evolution of the code to date.

At the beginning of this project the BATSRUS code contained ideal or resistive magnetohydrodynamics and included

- multispecies and multifluid MHD with ideal EOS
- explicit and fully implicit time discretization

- block-adaptive grid in 3D
- Cartesian, cylindrical and spherical grids.

During the first year of the CRASH project we added the following features:

- Non-ideal equation of state for high-energy-density plasma
- Numerical scheme for strong shocks with non-ideal EOS
- Using 1D or 2D HYADES output to set initial conditions for CRASH
- Tracking and solving for multiple materials
- Reading and interpolating tabular EOS and opacity data
- Gray diffusion radiation transport with flux limiter
- Semi-implicit time discretization (explicit hydro, implicit radiation)
- R-Z geometry in 2D.

The above features were discussed in our Year 1 Annual Report and have now been used for a year in CRASH 1.0. In the second year we have further developed the code to CRASH 2.0 with the following capabilities:

- Equation of state with separate electron temperature
- Calculated multi-group opacities
- Electron energy equation with semi-implicit heat conduction
- Radiative transport with multigroup flux-limited diffusion
- Synthetic radiographs both for 3D and for R-Z geometry including experimentally appropriate blurring and noise
- New Block Adaptive Tree Library (BATL) that provides
 - new capabilities such as 1D and 2D AMR, and
 - significantly more efficient dynamic mesh refinement in 3D.

We have also developed the CRASH preprocessors and postprocessors:

- HYADES 2D has an automatic remap algorithm.
- Physics Informed Emulator (PIE) for dimension reduction of the initial conditions in one dimension.
- Feature recognition software to identify shock location, wall shock angle etc. in experimental data and model output.

All of the components of CRASH 2.0 run independently and pass verification tests. The integration of these components is now complete; we will formally tag version 2.0 when needed for our UQ work. The following sections include examples in which combinations of these components are used. We anticipate the release of CRASH 2.0 within a few weeks. The following sections describe the major elements of CRASH 2.0 and the range of tests that are routinely used to confirm its continued correct performance.

In the following sections we discuss our progress during the second year, with some discussion of the next steps.

A. Equation of state and opacity model.

CRASH includes inline functions for the Equation Of State (EOS). The EOS used is for partially ionized ideal gases, in which the ionization equilibrium in a mixture of up to 6 components is calculated using the statistical sum method. The EOS functions are used in the course of the hydrodynamic simulations in order to recover the plasma pressure from the internal energy density, and *vice versa*.

Our opacity and EOS models are based on first principles with specified assumptions. We can use the model inline, but more typically use it to construct EOS and opacity tables that are then accessed by the flow solver. Alternative EOS and opacity tables could be used, but our approach gives us a consistency that is not typically available when using tabular EOS and opacity data, since the two are calculated under the same assumptions. Another advantage of our approach is that we have a finite list of input parameters for the model, specifically the

- ionization potentials
- excitation energies and multiplicities
- cross-sections
- oscillator strengths

This opens up the possibility of using these as inputs in an uncertainty quantification process, determining the sensitivity of our ultimate outputs to these elements of the EOS/opacity model.

The method is based on using the Helmholtz free energy to solve for the ionization equilibrium, with contributions from Fermi statistics in the free electron gas, Coulomb interactions, excited levels and pressure ionization. The internal energy density and the pressure are then expressed in terms of derivatives of the Helmholtz free energy. The effects of Fermi-gas statistics for the (ideal) electron gas are fully accounted for. In incorporating these effects into the model, we accordingly account for both the contribution to the pressure from the electron exchange effects and the reduction in the degree of ionization, resulting from the ionization equilibrium shift due to the increased electron pressure. During the past year we incorporated non-ideal plasma effects (i.e. the electrostatic interaction) into the model. In including the negative electrostatic energy $\sim Z^2 e^2/R$, where R may be the Debye length or the ion-sphere radius, into the Helmholtz free energy and then into the pressure, we accounted for the increase in the ionization degree, which may be properly described as an ionization potential decrease (“continuum lowering”) by $\sim Ze^2/R$. In comparing our model with the SESAME model for ionization, we find a deviation of ~ 0.2 .

Frequency-dependent absorption coefficients are calculated including the effects of Bremsstrahlung, photo-ionization of the outermost electrons, and bound-bound transitions with spectral line broadening. Multigroup opacities are then calculated by averaging the absorption coefficients over the photon energy groups.

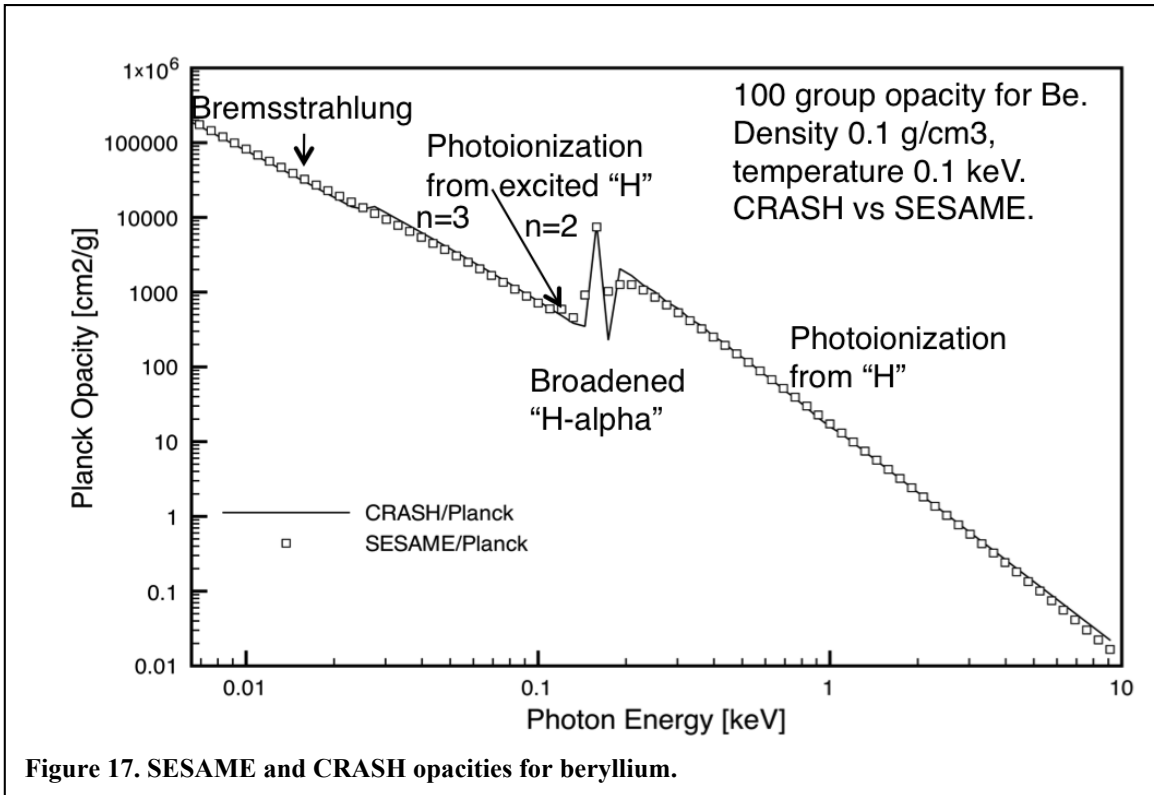


Figure 17. SESAME and CRASH opacities for beryllium.

B. Electron energy equation with semi-implicit heat conduction

We have implemented electron dynamics in the CRASH code. Under most conditions the electrons are very strongly coupled to the ions by collisions. However, for higher temperatures the electrons and ions get increasingly decoupled. At the shock front, where the ions are heated by the shock wave, the electron and ions are no longer in temperature equilibrium. Ion energy is transferred to the electrons by collisions. The electrons will in turn radiate energy.

The implementation of the electron equations is similar to that for gray radiation diffusion. The electron dynamics consists of two parts: advection and compression, which are solved explicitly, and electron heat conduction and thermal heat transfer between the ions and electrons, which are solved implicitly.

The electron pressure equation is a scalar advection problem. The force and work done by the electron pressure is added to the ion hydrodynamic equations. The combined hydrodynamic electron and ion equations are solved with either the HLLE or the Godunov numerical scheme. For the second-order Godunov scheme, we apply a limited

reconstruction together with an exact Riemann solver for constant polytropic index $\gamma=5/3$. We add up all pressures, including the radiation pressure, to have an upper bound for the speed of sound: $c_s^2 = \gamma p/\rho$. Afterwards we correct for the polytropic index of the isotropic radiation and the spatially varying polytropic index of the electrons. To account for the spatially varying polytropic index of the electrons, γ_e , due to ionization, excitation, and Coulomb interactions, we use the method of artificial relaxation. Here, we conservatively advect an extra internal electron energy, ΔE_e , as the difference between the true electron internal energy and the translational electron energy. At the end of the time step we recover the true electron internal energy: $E_e = p_e /(\gamma - 1) + \Delta E_e$. The electron pressure is recovered from the updated electron energy and mass density by either the inline electron EOS: $p_e = p_{\text{EOS}}(\rho, E_e)$ or the electron lookup tables.

The electron heat conduction and energy exchange between the electrons and ions are implicitly updated after the explicit hydro time step. The coupled system of ion and electron energy is of the form:

$$\begin{aligned} c_{vi} \frac{\partial T_i}{\partial t} &= \lambda_{ei}(T_e - T_i), \\ c_{ve} \frac{\partial T_e}{\partial t} &= \nabla \cdot [C_e \nabla T_e] + \lambda_{ei}(T_i - T_e), \end{aligned}$$

where T_i and T_e are the ion and electron temperature, c_{vi} and c_{ve} are the ion and electron specific heats, C_e is the electron heat conduction coefficient, and λ_{ei} is the electron-ion coupling coefficient. In combination with the gray or multigroup radiation diffusion, we find it convenient to linearize the coupled system in terms of aT_i^4 and aT_e^4 where a is the radiation coefficient. We freeze the coefficients while advancing the solution through a time step. The matrix system we solve has a symmetric, positive definite and diagonal-dominant matrix and can be solved by a preconditioned conjugate gradient method. After the implicit solve, we update the electron energy by $E_e^{n+1} = E_e^n + c_{ve}(T_e^{n+1} - T_e^n)$. The ion temperature is solved point implicitly. The implementation is generalized to use the infrastructure of the new AMR library BATL.

We have verified the heat conduction implementation with several tests to demonstrate convergence to analytical or semi-analytical solutions:

- 2nd order convergence of a 2D uniform heat conduction coefficient test in rz-geometry.
- The Reinicke Meyer-ter Vehn test in rz-geometry consisting of a self-similar, spherically symmetric blast wave with a leading heat front.
- A modification of one of the non-equilibrium gray diffusion tests of R. Lowrie, where the radiation energy is replaced by the electron energy and the hydro part of the problem is now formulated for ions only.

The original 1D solution of Lowrie is rotated by $\text{atan}(1/2)$ on a 2D AMR grid and advected orthogonal to the shock front. The heat conduction and electron-ion coupling

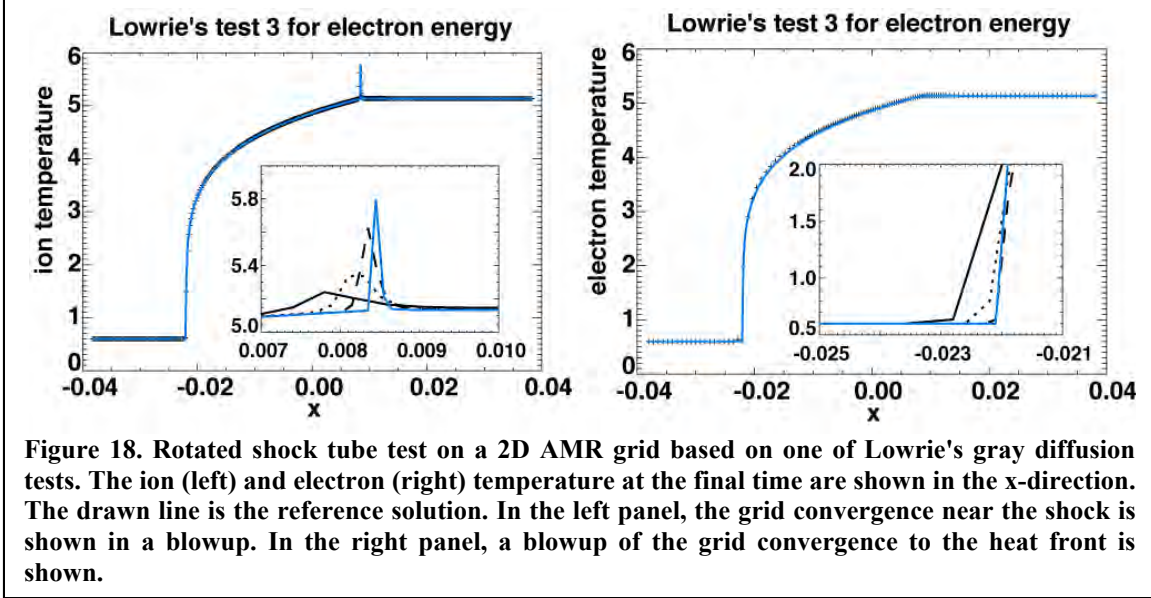


Figure 18. Rotated shock tube test on a 2D AMR grid based on one of Lowrie's gray diffusion tests. The ion (left) and electron (right) temperature at the final time are shown in the x -direction. The drawn line is the reference solution. In the left panel, the grid convergence near the shock is shown in a blowup. In the right panel, a blowup of the grid convergence to the heat front is shown.

coefficient are defined such that the electron-ion test problem is the same as the last test in R.B. Lowrie and J.D. Edwards.⁸ In our case, the non-uniform coefficients are defined in terms of the density and ion temperature. Figure 18 shows the ion and electron temperatures at the final time. The heat front at $x \sim -0.022$ is equivalent to the radiation precursor front in the gray diffusion model.

C. Radiative transport with multigroup diffusion

We have developed a multigroup-diffusion, radiation-transport module in the CRASH code. The advantage of having a multigroup solver in CRASH in combination with the electron energy equation is that this allows us to extend the initial HYADES simulation with the same types of dynamical equations in CRASH. More importantly, experience suggests that these capabilities represent the minimum level of physical fidelity that may be needed to accurately model the CRASH experiments.

As with the gray radiation diffusion model, the advection and compression of the radiation groups is solved explicitly. The force and work done by the total radiation pressure is added to the hydrodynamics equations. The multigroup solver is embedded in both the HLLE and Godunov numerical hydro solver. The HLLE scheme is stabilized by using the added radiation and kinetic pressure in the speed of sound used in the numerical diffusion. For the Godunov solver, we modify the exact Riemann solver for constant polytropic index $\gamma = 5/3$. We add the total radiation pressure to the gas kinetic pressure before applying the Godunov scheme to have an upper bound for the speed of sound. To correct for the polytropic index of the isotropic radiation, $\gamma_r = 4/3$, we use the fact that $4/3$ is the average of 1 and $5/3$, so that for each group the isothermal and adiabatic expansion of the radiation pressure are averaged to get the true expansion.

For the multigroup radiation, we additionally solve explicitly in an operator-split manner for the group frequency shifts due to the compression effect, given by

$$\frac{\partial E_g}{\partial t} = \frac{1}{3} \nabla \cdot \mathbf{u} \int_{\varepsilon_g} \frac{\partial(\varepsilon E_g)}{\partial \varepsilon} d\varepsilon.$$

Here ε and E_g are the photon and group energies for the G groups indexed by g and \mathbf{u} is the material velocity. The group interval ranges, ε_g , are chosen to be uniform in the frequency logarithm of the photons. The frequency shift is a linear advection problem.

The group diffusion and the relaxation between matter the radiation groups is solved implicitly in the third operator split step. The coupled system is of the form:

$$c_v \frac{\partial T}{\partial t} = \sum_{g=1}^G c \sigma_{a,g} (E_g - B_g),$$

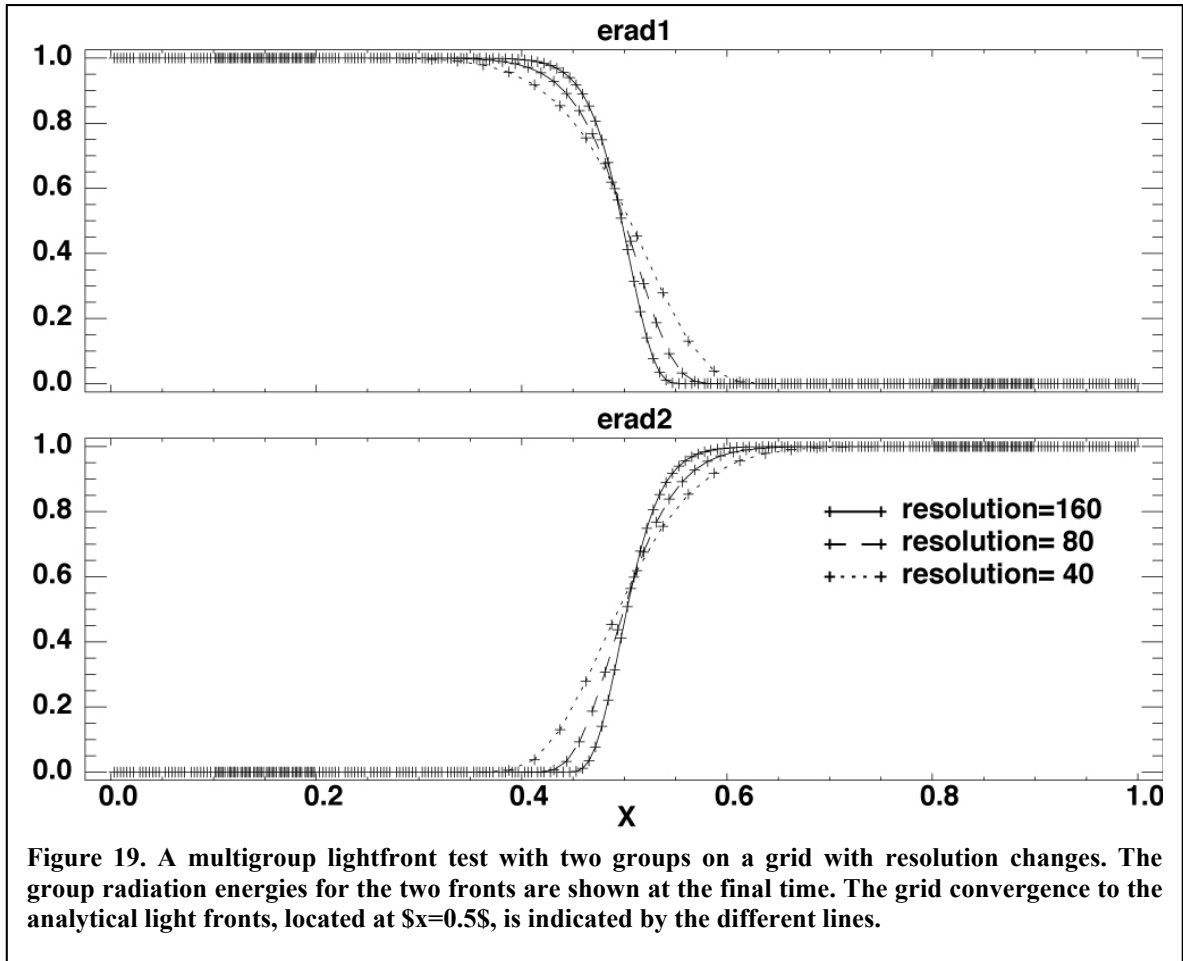
$$\frac{\partial E_g}{\partial t} = \nabla \cdot \left(\frac{c}{3\kappa_g} \nabla E_g \right) + c \sigma_{a,g} (B_g - E_g), \quad \text{for } g = 1, \dots, G,$$

where T is the electron temperature and B_g the group Planckian for the given temperature. The absorption coefficient, $\sigma_{a,g}$, is corrected to account for the stimulated emission and κ_g is the group Rosseland opacity. We added Larsen's squared radiation flux limiter as an option. This system is linearized and we employ the method of frozen coefficients. The linearized equations are iteratively solved by means of the GMRES method.

We have verified the multigroup implementation with several tests to demonstrate convergence to analytical solutions:

- An infinite-medium test with several radiation energy groups to check the material-radiation relaxation rate. The final equilibrium state has to be a Planckian energy distribution among the groups.
- A double lightfront test to check the group diffusion and flux limiters.

In Fig. 19, results of the multigroup light front test are shown in the x direction using two groups. The initial radiation energy is zero. The radiation energy for group 1 enters from the left boundary (see top panel), for group 2 it enters from the right boundary (bottom panel). Both fronts propagate with the speed of light. This is ensured by the flux-limiter in the flux-limited multigroup diffusion algorithm. The relaxation term between radiation and material is switched off, so that the two radiation groups evolve independently. Similar tests are performed in the y and z directions.

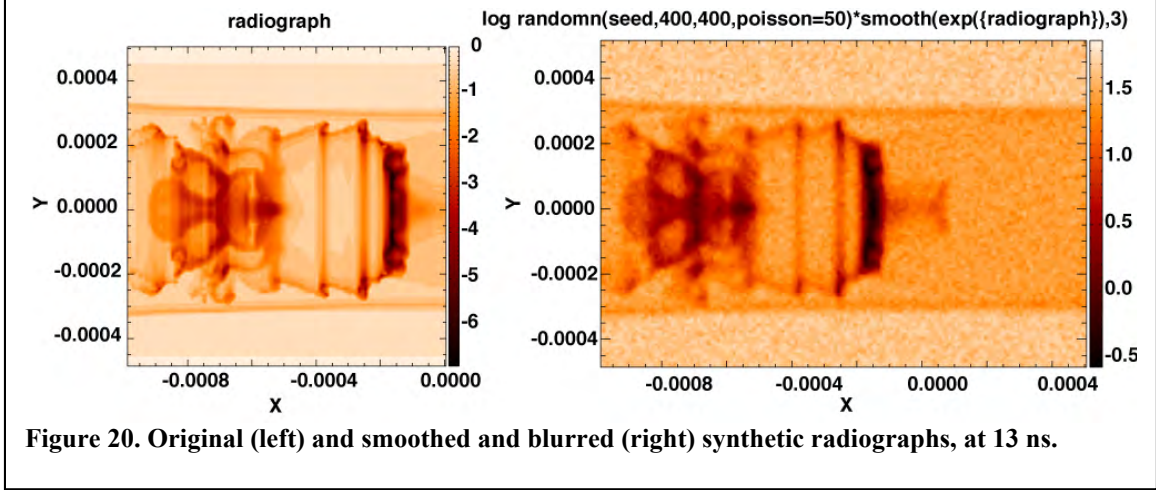


D. Synthetic radiographs

We have added the capability of generating synthetic radiographs at some required times during the simulation. We have also implemented experimentally appropriate blurring and noise, as recommended by the October 2009 review. The plotting times, the location (or possibly locations) of the X-ray source(s) and the orientation, size and number of pixels of the radiograph image(s) are given as input parameters. The optical depth is an integral of the density multiplied by the opacity characteristic for the material and the spectrum of the X-ray source along the ray:

$$D = \int_0^{\infty} \rho \kappa(m) dl$$

The ray is a straight line from the X-ray source to the center of the image pixel. We assume that the absorption is dominated by the X-ray line near 5.18 keV and the opacities at this energy $\kappa(m)$ for material m are 79.4, 0.36 and 2.24 m^2/kg for Xe, Be and polyimide, respectively. The contribution from scattered X-ray photons is neglected.



The parallel algorithm works the following way. For each ray and each grid block we determine the segment of the ray (if any) that intersects the block. Then we integrate the above formula using a trapezoidal rule and second order trilinear interpolation. The step size is proportional to the cell size of the block. In R-Z geometry the blocks correspond to rings with a rectangular cross section. The ray can intersect the ring at at most 4 points forming at most two segments inside the ring. The integration is done along the segment(s) in 3D space, but $\rho\kappa_m$ is obtained with bi-linear interpolation in 2D corresponding to the R-Z coordinates. Once the integration is done for all grid blocks, the partial integrals are added up using an `MPI_reduce` call.

The algorithm is verified by an analytic problem where we integrate through a sphere of a given non-trivial density profile. Second order convergence towards the analytic solution has been verified both for 3D Cartesian and 2D R-Z non-uniform grids.

We use the synthetic radiograph images to compare with experimental data. To make the images more comparable, we need to take into account the finite size of the X-ray source (about 20 μm diameter), the finite length of the X-ray pulse (about 0.2 ns) and the Poisson noise due to the finite number of photons (about 50 photons per 100 μm^2 image pixel). The first two effects can be approximated by smoothing the synthetic image with a characteristic length of 20 to 26 μm (or 2 to 3 pixels), while the Poisson noise can be taken into account as

$$D' = -\log[P(50) \exp(-D)] = D - \log P(50)$$

where P is a random number with a Poisson distribution and a mean value of 50. Figure 20 shows a comparison between the original synthetic radiograph and the "smoothed and blurred" radiograph.

E. Block Adaptive Tree Library

We have developed a completely new Block Adaptive Tree Library (BATL) that has several new capabilities relative to the original block-adaptive code in BATSURUS, and it is also more accurate and efficient for some problems. In particular BATL can

- handle truly 1D and 2D adaptive grids with a single grid cell in the ignored directions
- adapt the grid in only some of the dimensions
- do grid adaptation and load balancing in a single step
- do conservative grid adaptation and flux correction in R-Z geometry
- interpolate ghost cells in time when local time-stepping is used in time-dependent problems

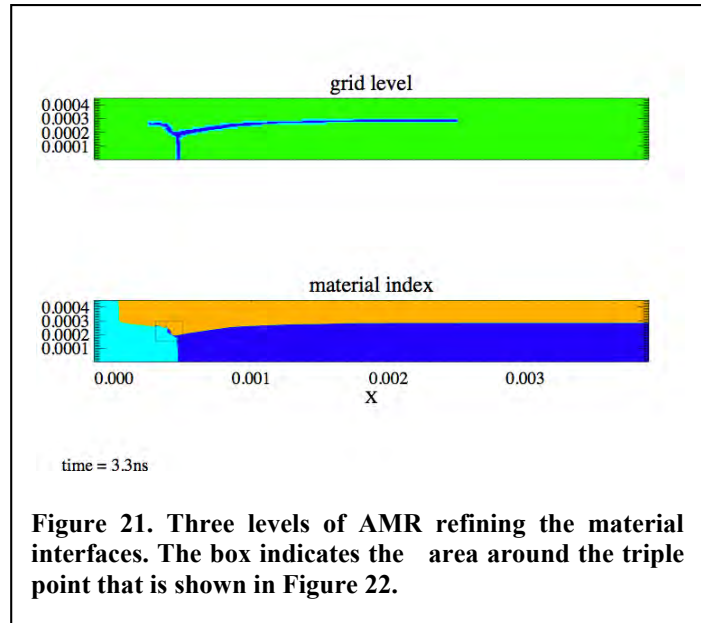


Figure 21. Three levels of AMR refining the material interfaces. The box indicates the area around the triple point that is shown in Figure 22.

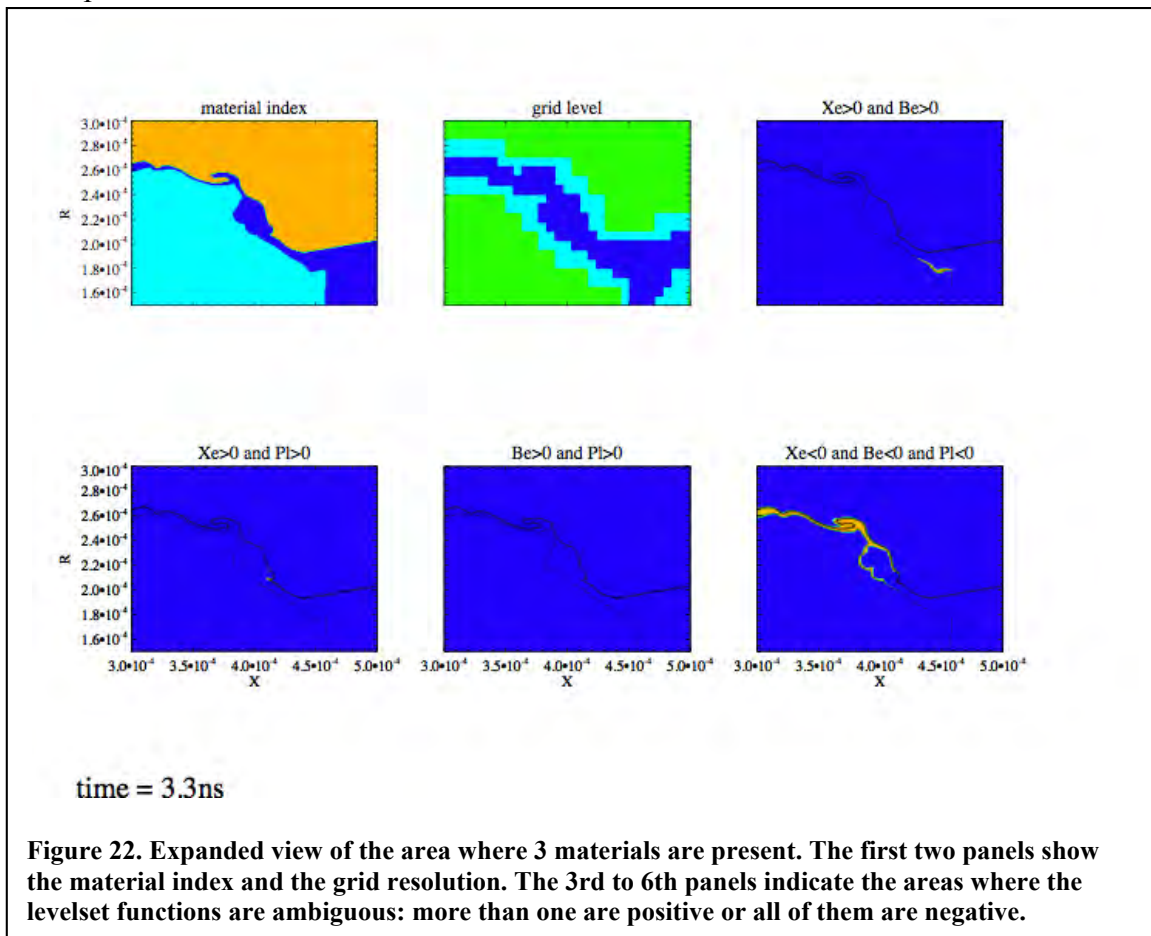


Figure 22. Expanded view of the area where 3 materials are present. The first two panels show the material index and the grid resolution. The 3rd to 6th panels indicate the areas where the levelset functions are ambiguous: more than one are positive or all of them are negative.

BATL is written as a self-contained library with an object-oriented design. All modules contain unit tests, and there is also a functionality test that demonstrates the advection of a circle/sphere with dynamic grid adaptation in various numbers of dimensions. BATL is a fully verified, efficient and flexible block adaptive tree library. Currently it consists of about 6000 lines of Fortran 90 code.

We have modified BATSRUS so that it can optionally use BATL instead of the original BATSRUS AMR code. We also modified BATSRUS to allow for 1D and 2D grids. Eventually we will extend BATL to cover all the tasks that BATSRUS requires (handling magnetic fields, spherical geometry, etc), so that we can switch to BATL completely. Our first priority was to cover all the functionality required for the CRASH simulations. This has been achieved, and now all CRASH tests use BATL.

BATL allows us to do highly resolved CRASH simulations efficiently. With the original code, the dynamic grid adaptation used to take up around 80% of the wall clock time in 3D AMR CRASH runs (grid adaptation is performed every time step); the original code was developed for problems requiring much less frequent adaptation. Using BATL the grid adaptation and load balancing uses only about 7% of the simulation time only. We can now do 2D R-Z geometry runs with 4500 x 1000 effective resolution on 16 cores in about 9 hours.

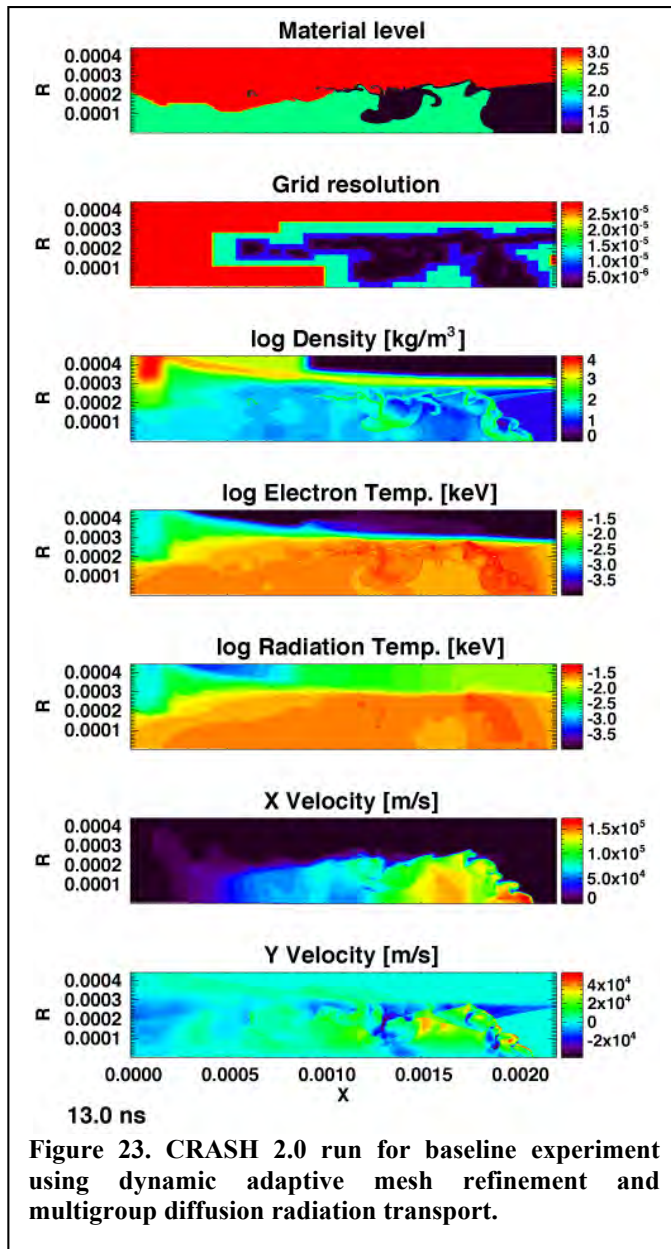


Figure 23. CRASH 2.0 run for baseline experiment using dynamic adaptive mesh refinement and multigroup diffusion radiation transport.

Figure 21 shows how we can resolve the material interfaces (and the shocks) using grid adaptation. The blocks contain 4x4 grid cells. Figure 22 shows a detailed view near the triple point where all three materials are present. The grid adaptation can reduce the ambiguity of the levelset functions (due to numerical errors) to an area that is much smaller than the width of the Xe layer penetrating between the Be and plastic.

F. Run results with CRASH 2.0

We are in the process of integrating the new capabilities of CRASH 2.0, all of which function and pass appropriate tests independently. We have done several runs using various combinations of the new capabilities. Figure 23 shows results that employ multigroup-diffusion radiation transport and 2D AMR in R-Z geometry. We are working actively on completing the integration of these new capabilities.

G. Parallel Deterministic Transport (PDT)

The TAMU PDT code represents our highest fidelity radiation model. We have made substantial progress on improvements to the PDT code, described below, have defined the interface required to couple PDT to BATSRUS, and have done some testing of some elements of the interface. However, we chose to prioritize both the multigroup diffusion capability and the improvements to PDT required for its effective use in UQ calculations above completion of the coupling during the past year. Our 2009 review and the associated report brought forward two points of view. On the one hand, multigroup diffusion may be sufficient for our problem. On the other hand, if we really need PDT then it is important to get the coupled code running relatively soon. However, we have since realized that we can assess the importance of coupling BATSRUS to PDT by running identical test radiative transport problems, modeled after the full CRASH problem, independently in PDT and BATSRUS. This is now a high priority. The next few paragraphs summarize areas of progress with PDT during the past year.

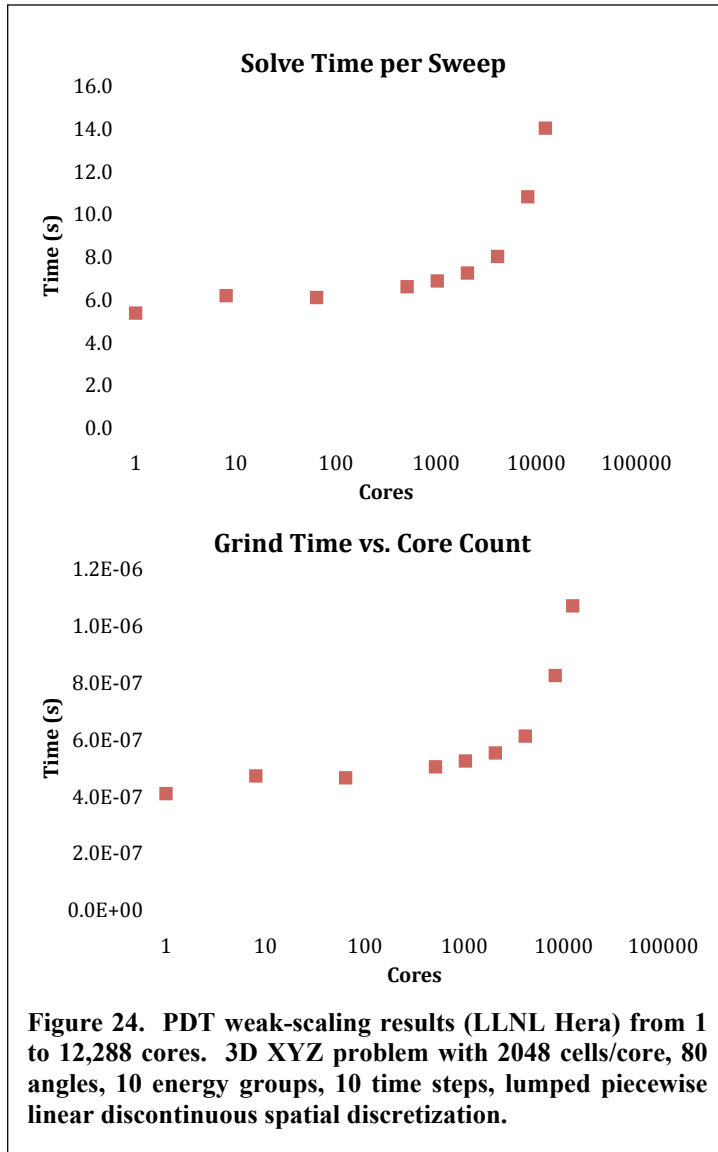
Thermal Radiation Transport Solver: During the most recent project year we have focused significant effort on enhancing the performance and robustness of the thermal radiation solver. We have implemented an adaptive time step algorithm that has broadened the set of problems that the code can readily solve. We have implemented and tested various options for the time-centering of material properties, including an option for full implicit updating of the opacities as well as the Planckian emission term. We have improved our algorithm for robustly handling negative electron and radiation temperatures. We have added a general source treatment that will allow flexible specification of material heat sources and radiation-emission sources, which will enable us to run a wide variety of verification problems including those with manufactured solutions. We are also adding various initialization options for angular intensities and material temperatures, including the option of reading them from a re-start file. Finally, work is well underway on the implementation of a diffusion solver for a gray diffusion preconditioner that will accelerate multifrequency transport iterations. Without preconditioning, our Krylov methods enable solution of difficult problems, but the solution of such problems is expected to be much more efficient with the preconditioner.

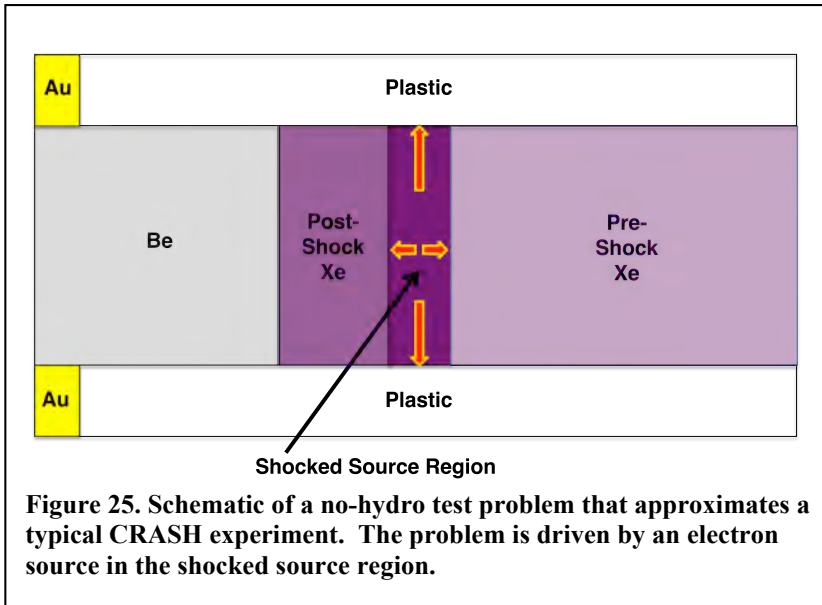
Performance: The computational demands of a full transport calculation are high enough that every increase in efficiency (accuracy per unit computational resource) will increase the value of the PDT transport capability to our project. With this in mind, the PDT development team has devoted considerable effort to both the serial and parallel performance of the code. We have been very successful in improving the performance of discontinuous finite-element spatial discretization methods, reducing the solve time per

unknown by a factor of approximately thirty. In addition, we have implemented a new I/O model to help scale to large core counts, and we are conducting scaling studies to further identify and correct parallel scaling issues (See Fig. 24).

STAPL: The current version of PDT is built on the Parallel Transport Template Library (PTTL), which is a predecessor to the Standard Template Adaptive Parallel Library (STAPL) that is being created by the TAMU Computer Science team. PTTL has several known limitations, including some that affect scaling and others that limit flexibility. The Comp-Sci team has been working throughout the project to generate version 1 of the STAPL library, and they have recently completed this task to the point that we can now begin to port PDT from PTTL to this newly emerging STAPL. We will devote considerable effort to this porting during the coming year. This will enable PDT to scale to larger processor counts and will make it straightforward to add capabilities for 2D axisymmetric calculations and calculations with reflecting boundaries.

2D Capability: During the most recent project year we have expanded and tested the 2D Cartesian (x,y) capability in PDT, which now successfully runs radiative transfer test problems. We have also made progress toward a 2D axisymmetric (r,z) capability, which is expected to be the workhorse for most CRASH/PDT simulations. A significant difference in (r,z) transport is that during the "sweeping" phase, the solution in a given direction depends on the solution in other directions. Previous versions of PDT assumed independence (which is true for Cartesian problems) and exploited it in its parallel execution. With the new STAPL, it will be much more straightforward (than it would be with PTTL) to enforce the dependencies that are demanded by the axisymmetric sweep.

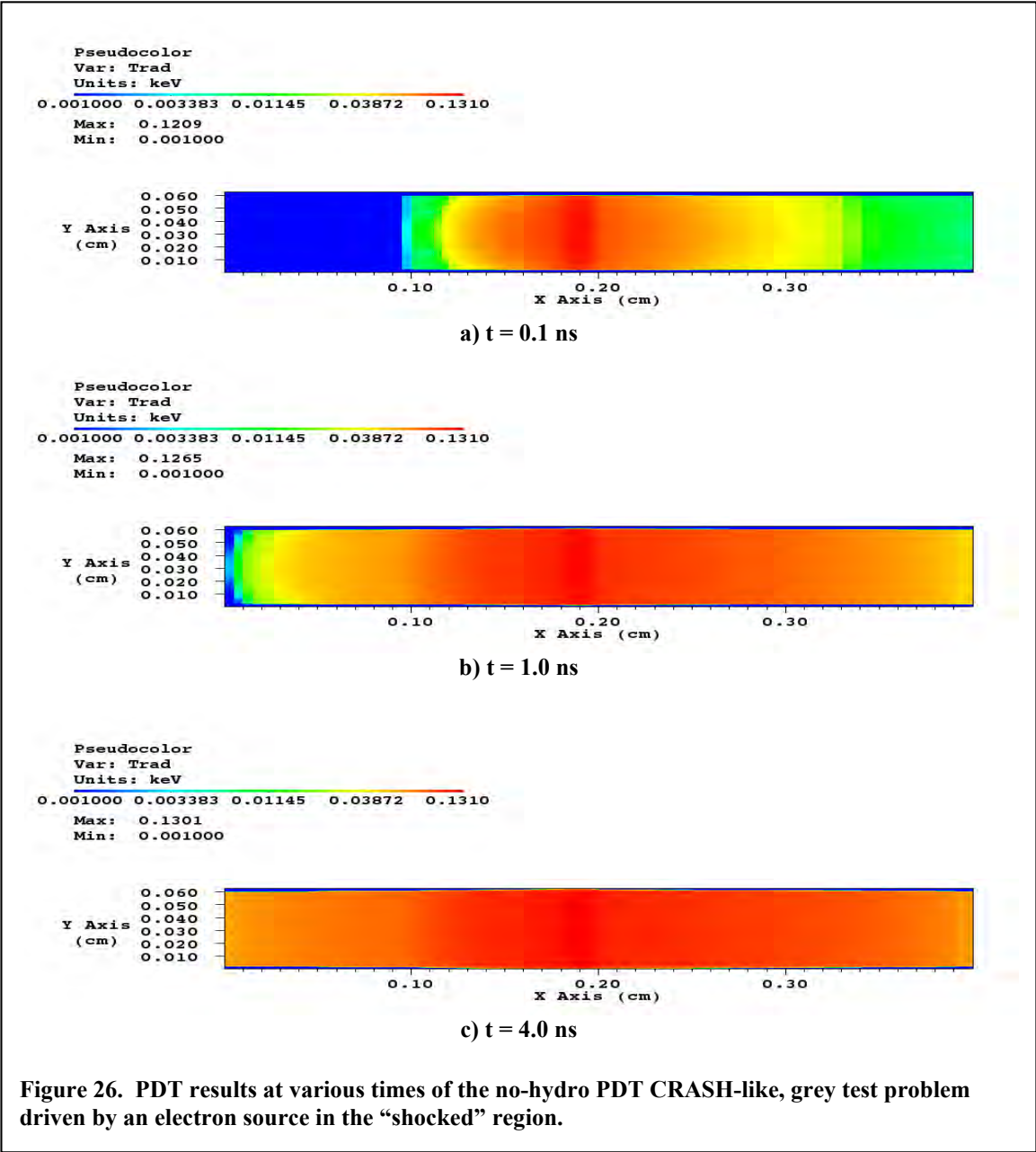


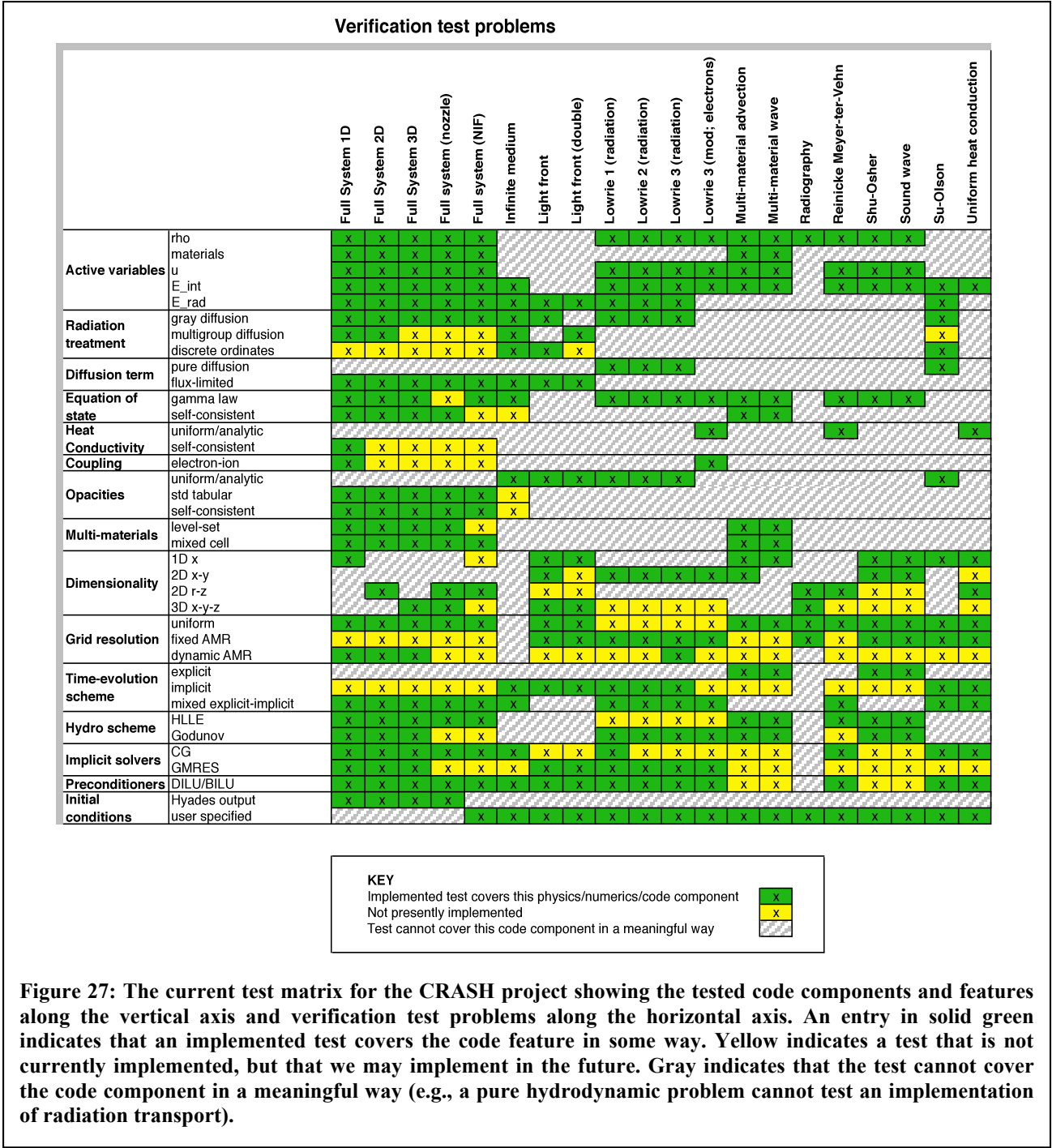


Accomplishing this and thus creating an (r,z) capability is a high priority for the PDT team in the coming project year.

Test Problems: We have added various Su-Olsen test cases to our regression test suite, and we continue to develop problems with manufactured solutions. We have also devised no-hydro test problems that

approximate a typical CRASH experiment viewed in the reference frame of the shock. See Figure 25 for a schematic of a no-hydro test problem, and Figure 26 for a sampling of PDT results. These problems will help us assess differences among radiation treatments ranging from gray diffusion to multi-frequency transport, as a function of frequency-group structure, spatial resolution, and angular resolution. These assessments will feed into the uncertainty quantification of our CRASH simulations.





H. Software testing and verification: Test Matrix

We have made significant advances on code testing within the CRASH project in the past year. These advances include progress in both the number of lines of code covered by regression tests and in the maturing of strategies for code verification.

The addition of specific tests is motivated by additions and modifications to the code. The overarching testing strategy is motivated by diverse viewpoints, which lead to diverse testing strategies and, ultimately, to a diverse collection of tests (see below). These viewpoints include:

- A scientific modeling viewpoint, which leads to testing the implementation of terms and sets of terms from the fundamental equations of the models.
- A software-development viewpoint, which leads to testing the implementation of individual and collective subroutines and functions.
- A feature-based viewpoint, which leads to testing the implementation of code features.
- A user viewpoint, which leads to testing based on experiences with the code, especially applying tests based on unexpected code behavior.

Over the past year, capabilities of the CRASH code have been added or enhanced. This has led to additional testing in the various modules. Key additions include

- Multi-material advection
- Heat conduction with uniform diffusion
- The Reinicke & Meyer-ter-Vehn problem
- Lowrie test 3 for electron heat conduction (discussed above)
- Light-front propagation: flux-limited diffusion and discrete ordinates (the latter using PDT)
- Multigroup, flux-limited-diffusion, light-front propagation (see above)
- Su-Olson problem for propagation of a Marshak wave
- Matter-radiation equilibration of an infinite medium
- Simulated radiography for simple shapes having analytic solutions and for shock-tube images in 2 and 3D.

Figure 27 shows the current test matrix for the CRASH project. Tested code components and features are arrayed along the vertical axis with verification test problems along the horizontal axis. Each verification test has quantitative pass/fail criterion. As part of the testing procedure, each covered solution component (shown in green in the figure) is set up to enable a convergence study. These are performed to test for grid and/or time

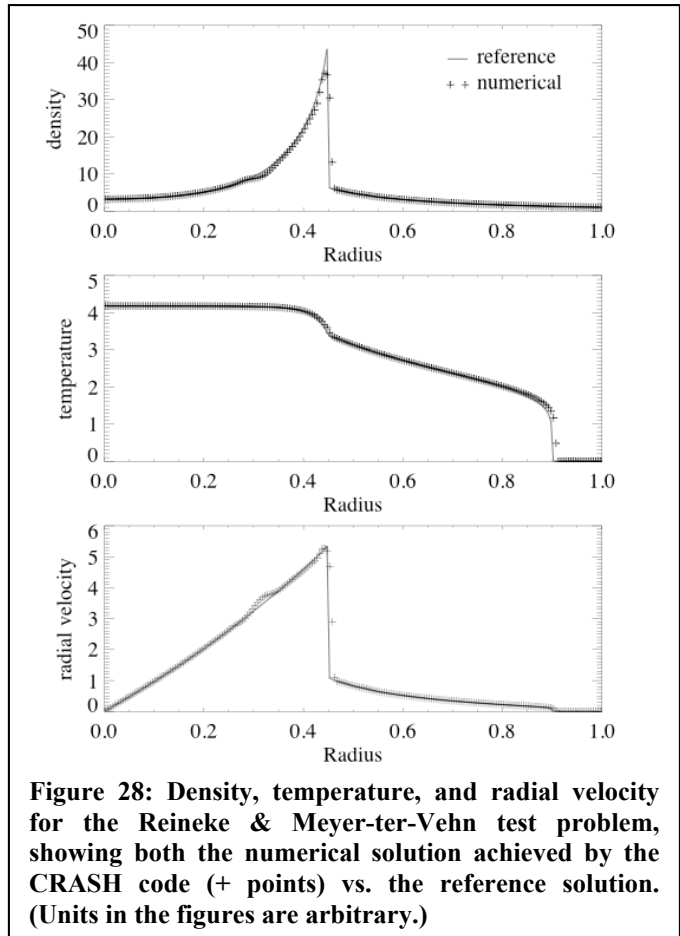


Figure 28: Density, temperature, and radial velocity for the Reineke & Meyer-ter-Vehn test problem, showing both the numerical solution achieved by the CRASH code (+ points) vs. the reference solution. (Units in the figures are arbitrary.)

convergence, as deemed appropriate. Provision is also made for parallel scalability studies, in such test problems where the scope of the problem makes this meaningful.

In the sections that follow we highlight some specific verification tests implemented since the last review.

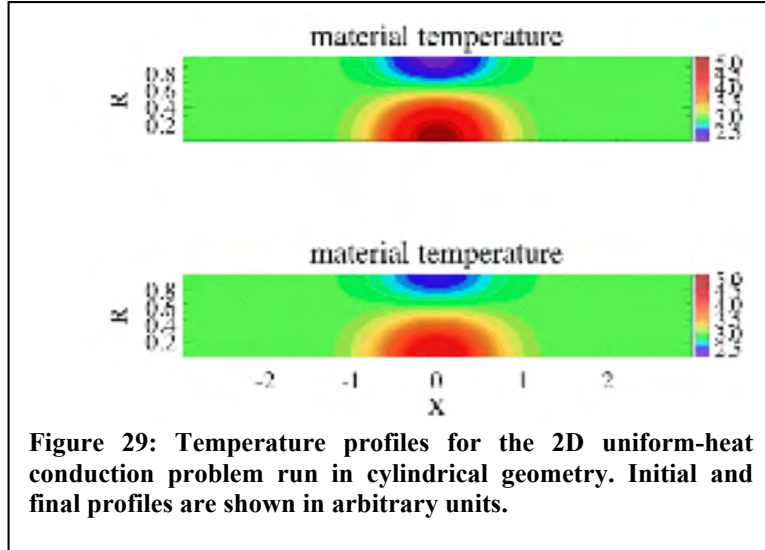


Figure 29: Temperature profiles for the 2D uniform-heat conduction problem run in cylindrical geometry. Initial and final profiles are shown in arbitrary units.

a. Reinicke & Meyer-ter-Vehn

The Reinicke & Myer-ter-Vehn problem is a test of both hydrodynamics and heat conduction. It extends the familiar Sedov–Taylor blast-wave problem with the addition of heat conduction through a parameterized heat conductivity proportional to $\rho^a T^b$. There is an initial “bomb” of energy placed at the origin of the domain. Similar to Sedov–Taylor, an expanding shock front is produced. However, in this case, thermal conduction dominates the fluid flow, and a thermal front precedes the hydrodynamic shock. A self-similar solution exists to the problem, against which we compare our numerical solution. Results versus the reference solution are shown in Figure 28. Note that, given the dominance of the shock in this problem, only first-order spatial accuracy is expected and achieved.

b. Uniform heat conduction

The problem of uniform heat conduction provides a fundamental test of the implementation of electron heat conduction. It tests the diffusion in time of thermal profiles using constant and uniform heat conductivity. In the CRASH test suite, the problem is implemented in both 1 and 2 dimensions—in 1D, in slab geometry, where a Gaussian profile is evolved; in 2D, in r - z geometry, where the evolved profile is a

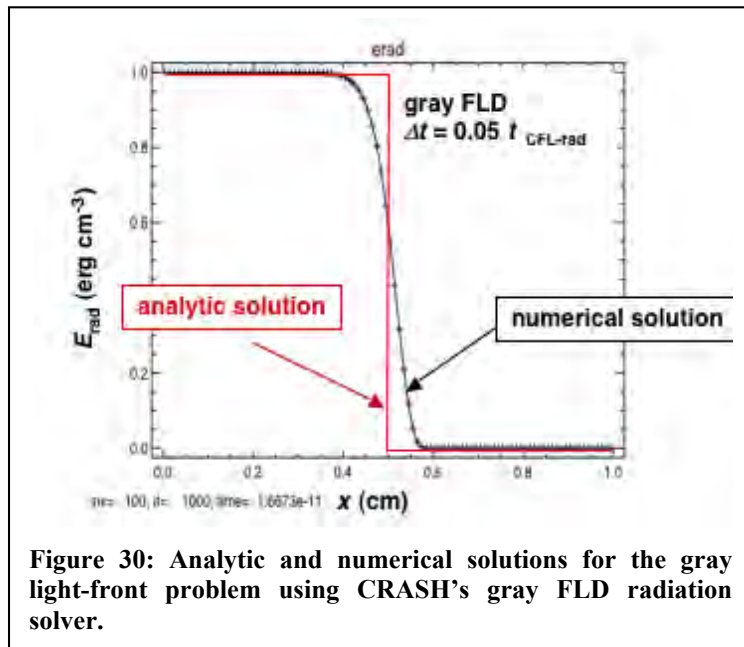


Figure 30: Analytic and numerical solutions for the gray light-front problem using CRASH’s gray FLD radiation solver.

Gaussian in the z direction and J_0 in the r direction. For testing, we use a Crank–Nicolson scheme for time evolution and are able to achieve second-order time accuracy. Second-order accuracy is also seen spatially. The temperature profile for the 2D problem is shown in Figure 29 at the initial and final times.

c. Light-front propagation

Propagating a light front correctly is perhaps the most fundamental test for any radiation solver. The CRASH verification test suite implements several versions of the light-front problem. This serves to test implementations of the radiation solvers (the approximate flux-limited diffusion (FLD) schemes, gray and multigroup, and discrete ordinates in anticipation of PDT/BATSRUS coupling). In addition to testing the radiation solver, it also serves to test the flux-limiting scheme used by the FLD solutions. The multigroup test was discussed above.

Propagation of light fronts is a challenge for FLD-based codes, since the behavior of the (more accurate) Boltzmann equation in this regime is hyperbolic and is the regime where the diffusion operator is least accurate. The problem is initialized by setting radiation-energy density in the computational domain to zero. A boundary condition at the origin of a finite radiation-energy density serves to inject radiation into the domain as time advances. The test is judged successful if the center of the evolved front propagates at speed c and that the spreading of the front is deemed sufficiently small. Figure 30 shows results for CRASH’s gray FLD solver using (first order accurate) backward Euler differencing.

d. Su-Olson problem

A natural extension from light-front propagation is the Su-Olson problem, where one propagates a light front but, in addition, there is matter–radiation energy exchange. The problem is linearized, with the specific heat proportional to T^3 . CRASH implements this in slab geometry and solves the problem in two ways: (i) with radiation- and matter-energy density solved together and self-consistently and (ii) with the radiation-energy density solved alone and the matter energy adjusted to maintain energy balance. In both cases, comparison to the reference solution is very good, and second-order accuracy in both space and time is achieved. Figure 31 shows the results.

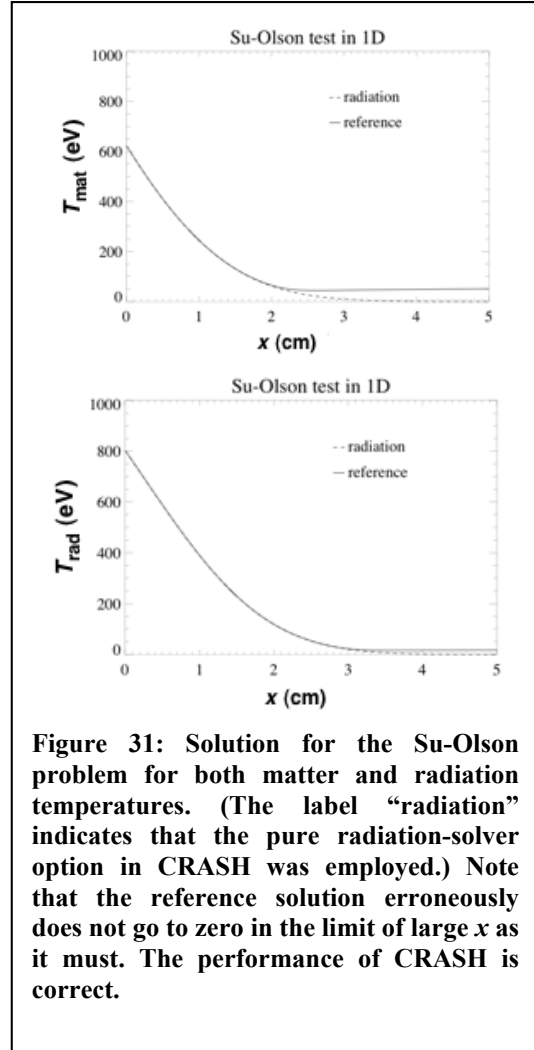


Figure 31: Solution for the Su-Olson problem for both matter and radiation temperatures. (The label “radiation” indicates that the pure radiation-solver option in CRASH was employed.) Note that the reference solution erroneously does not go to zero in the limit of large x as it must. The performance of CRASH is correct.

IV. Experiments

The CRASH team has executed two experiments at the Omega laser facility. The most recent experiment, the Year 2 experiment, was in December of 2009. The Year 2 experiment aimed to characterize the initial conditions of the radiative shock experiment. The CRASH code requires calibrated input from HYADES for the laser-driven state; the goal of the Year 2 experiment was to acquire the data needed for the calibration. Also, data from the Year 1 experiment, acquired in October 2008 has been analyzed. The Year 1 experiment focused on the repeatability of the radiative shock experiments.⁵ The results of this analysis have been published⁵ by CRASH graduate student Forrest Doss in the journal *High Energy Density Physics*.

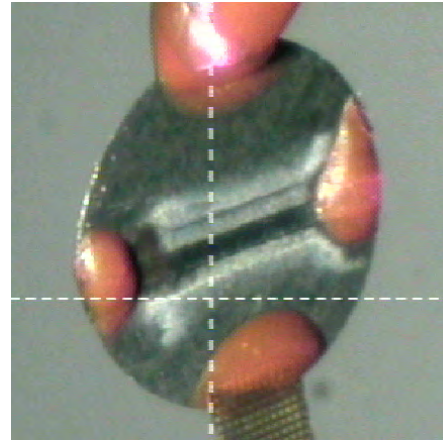


Figure 32. A picture of a stepped target with 5 and 10 μm laser-etched slots. VISAR and SOP were used to diagnose the breakout from the different thicknesses of Be. The pink globules on the disk are reinforcing glue.

The CRASH Year 2 experimental campaign included 13 shots. The main diagnostic was

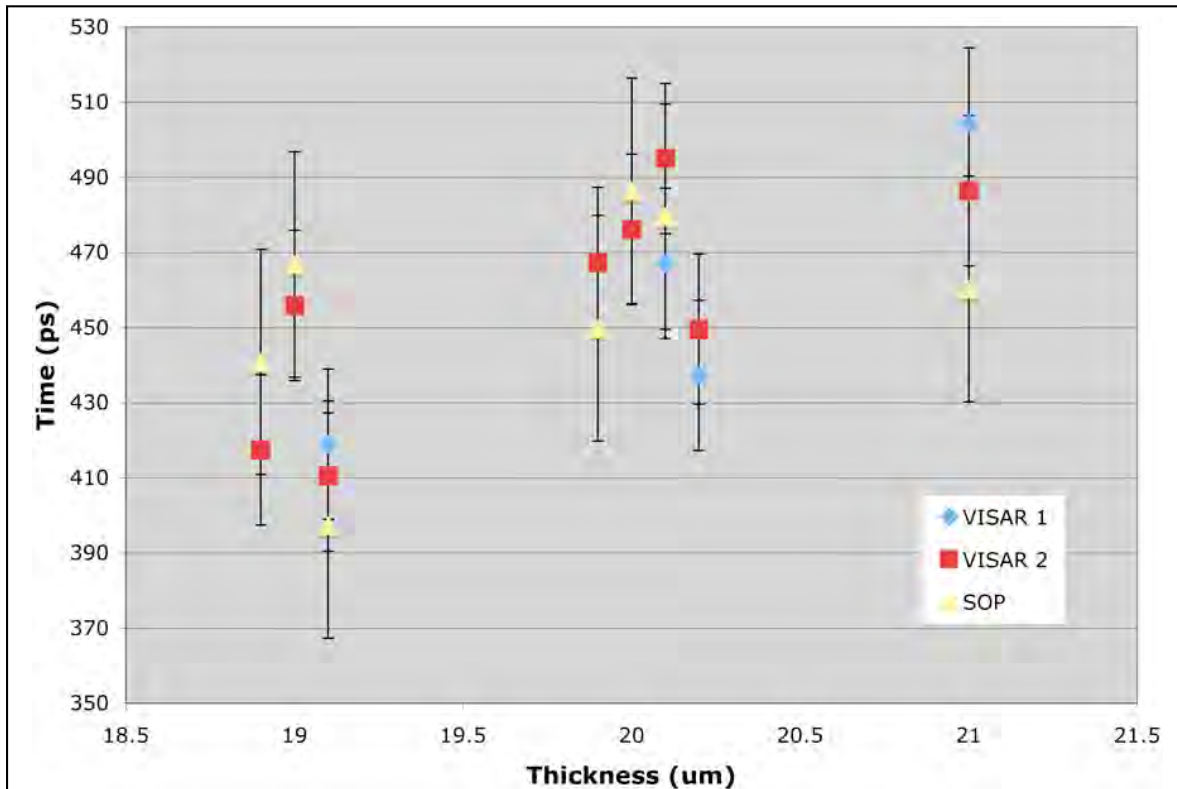


Figure 33. Shock breakout time versus Be disk thickness. Data from VISAR and SOP are shown. Disks were either 19, 20, or 21 μm , to within $\pm 0.5 \mu\text{m}$. Data points are offset to show individual shots.

a Velocity Interferometer by Any Reflector (VISAR), which detects the rate of change of optical path, and a Streaked Optical Pyrometer (SOP), which records thermal emission. The experimental campaign used 4 types of targets. One type was a nominally a planar Be disk with a thickness of nominally 20 μm and another type of target was a Be disk with 2 laser-etched slots. The slots had nominal thicknesses of 5 μm and 10 μm and a slotted or stepped disk is shown in Figure 32. The amount of material removed from the disk was measured with an error of $\pm 0.5 \mu\text{m}$. Combined with the error from measured total thickness of each disk the total error in thickness of the laser-etched slots was $\pm 1.1 \mu\text{m}$. Of the 5 disks that were used in the experiment the thickness of the nominally 10 μm slot ranged from 8 μm to 12 μm with an average of 9.6 μm and a variance of 2.3 μm . For the nominally 5 μm thick slot the average thickness ranged from 3.5 μm to 5.5 μm with an average of 4.7 μm and a variance of 0.83 μm .

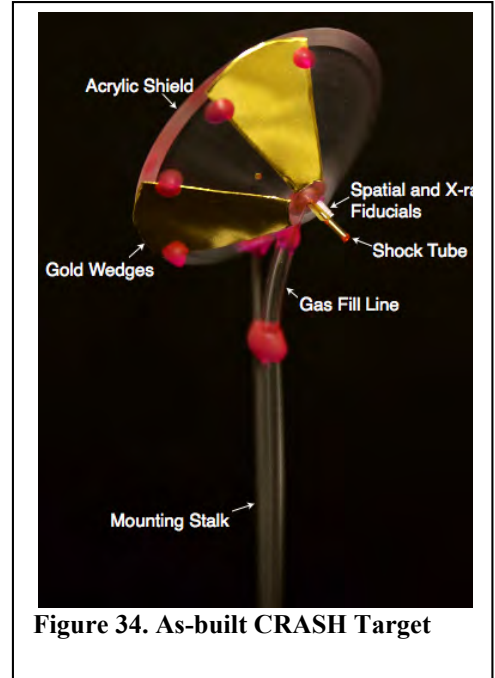


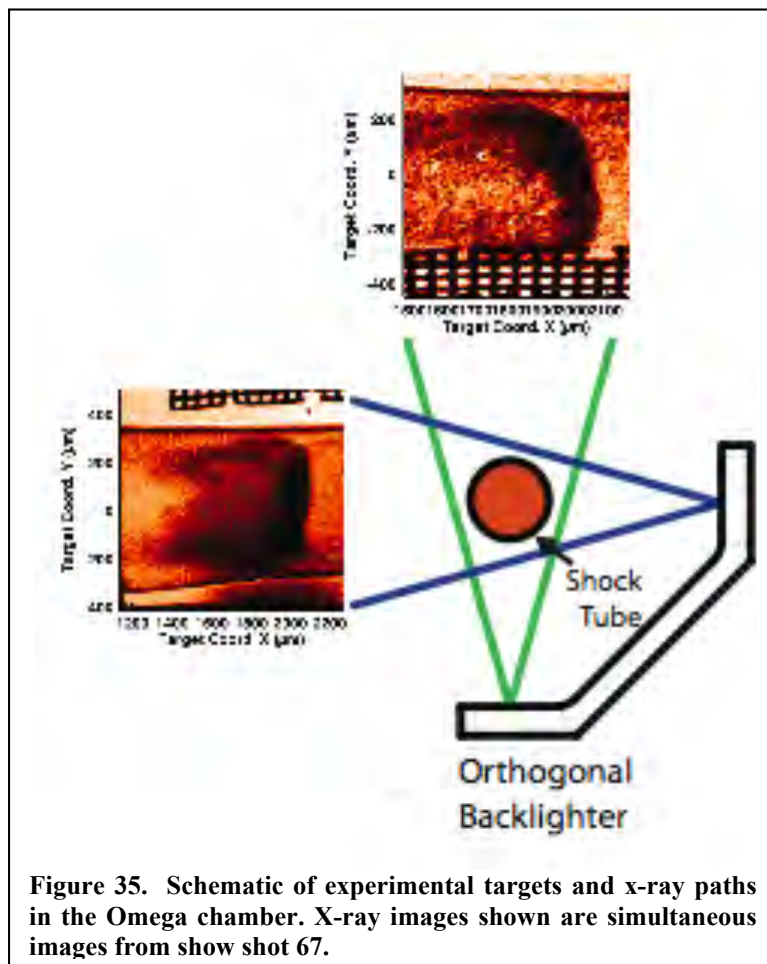
Figure 34. As-built CRASH Target

The majority of the data from the disk shots is analyzed and shown in Figure 33. It shows shock breakout time versus the disk thickness from one or two of the VISAR diagnostics and from the SOP. Disks were measured to be 19, 20 or 21, with an uncertainty of $\pm 1 \mu\text{m}$. The target thicknesses are offset by 0.1 μm from one another to make the plot clearer. The error in the time measurements from the VISAR diagnostics is $\pm 20 \text{ ps}$ and due to spreading of the signal the error in the measurements from the SOP diagnostic is $\pm 30 \text{ ps}$. In addition, there is a systematic uncertainty in the relative timing of the diagnostics and the drive lasers of $\pm 50 \text{ ps}$, not shown on the figure. Horizontal error bars from the thickness of the disks are not included in Figure 33. The analysis of the breakout from the nominally 5 μm and 10 μm slots are ongoing.

The other two targets in the Year 2 experiment were for more complex experiments. One was a gas-filled target with a thin polyimide window on the end of the tube. This would allow the VISAR beam to potentially reflect off of the shock, which due to the large pressure should be reflective, yielding a velocity trajectory for the shock. The fourth target type used the SOP to diagnose the shock while observing the shock from the side. This was an attempt to view the motion of the thermal emission from the shock, potentially giving the velocity of the shock. The analysis of these experiments is ongoing.

The CRASH Year 1 experimental campaign comprised of 11 shots. Figure 34 shows one of the targets. The targets were all nominally identical variations on a single design, intended to quantify aspects of experimental repeatability related to target manufacturing and experimental execution. A target consisted of a $21 \pm 1 \mu\text{m}$ Be disk mounted on a $625 \mu\text{m}$ OD polyimide tube. The tube was filled with Xe gas to a pressure of $1.14 \pm .04 \text{ atm}$, inserted into the Omega chamber, and then driven by 10 laser beams delivering $3.8 \pm .077 \text{ kJ}$ in a 1 ns pulse to the Be disk surface. Primary diagnostics for the Year 1 experiments were orthogonal x-ray radiography. The experiments were imaged at nominally $13 \pm 0.25 \text{ ns}$ ($0.25 \pm$ is the typical uncertainty, but occasionally it is $\pm 0.5 \text{ ns}$) after the drive. Backlighter illumination times were varied slightly through the day. Four shots were timed with 1 ns spacing. A vanadium point-projection pinhole backlighter was used to create 5.2 keV KeV x-rays, suitable for imaging the shocks. The x-ray data was captured on ungated x-ray film. Examples of typical radiographic data and for a schematic of the positions of the detectors, main target, and backlighters are shown in Figure 35.

Fifteen targets were constructed, of which the 11 most closely matching the construction specifications were used in the campaign. The location of the shock had a shot-to-shot variation of approximately 5%, conceivably stemming from the 5% uncertainty in Be drive disc thickness.

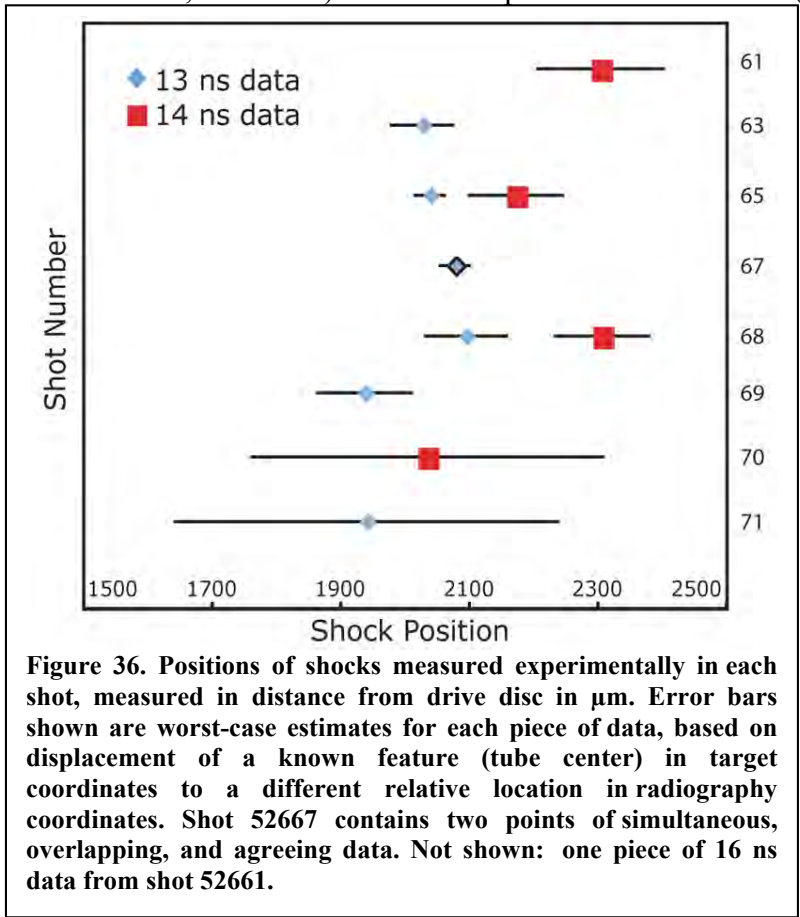


The shock positions are shown in Figure 36 for 10 shots. Post-shock dense layer widths were used to infer density compression ratios of $17 \pm 5 / -1$, confirming our presence well within the radiative collapse regime of compression greater than ~ 10 . Wall shock analysis³ implied an average shock Mach number relative to the precursor of 3.1, and average wall shock amplitudes of $70 \mu\text{m}$. The errors on Mach number and wall shock extension measurements are ± 0.1 and $\pm 9 \mu\text{m}$, respectively, with shot-to-shot variations of ± 0.16 and $\pm 14 \mu\text{m}$.

At the annual review in October 2009, the review team inquired about the quality of our experimental targets. It was suggested that we exchange information with other target fabrication facilities, specifically General Atomics. Recently, we have begun such an interchange of information. We recently co-assembled HED targets with LLNL for a Kelvin-Helmholtz instability experiment performed on the Omega laser facility. Freddy Hansen, a General Atomics employee and PI of the experiment, used the University of Michigan metrology station to metrologize the targets. Freddy has considerable experience executing HED experiments, which includes target metrology. Freddy has written a detailed comparison of the LLNL system and the Michigan system and has suggested improvements for both systems. The majority of the suggestions for Michigan were to make the system easier to use. However, some changes, such as increasing the magnification on the main camera and using a colored light filter could increase the accuracy of measurements. Michigan students are currently working on implementing some of the suggested changes.

V. Educational Status and Plans

Our current roster of graduate students associated with the CRASH center come from six departments at Michigan (Aerospace Engineering; Atmospheric, Oceanic and Space Sciences; Applied Physics, Nuclear Engineering and Radiological Sciences; Mathematics; Statistics) and two departments at TAMU (Computer Science, Nuclear



Engineering). Students are funded directly by the grant, by fellowships from cost-sharing, and by other fellowships or grants but doing research supported at least in part by CRASH. Several students have previously spent one or more summers at an NNSA lab. Two students visiting the labs in 2009, and we are working on setting up 2010 visits for several students (see Table 6).

Table 6. Students seeking to spend time at an NNSA lab in 2010.

Student	Lab	Contact
Channing Huntington	LLNL	Bruce Remington
Dave Starinshak	LLNL	Brian Spears
Hayes Stripling	LLNL	Pieter Dykema
Daniel Zaide	Pending	Pending

Students, besides meeting with their individual advisors, attend meetings of the group roughly every two weeks. These meetings consist of a mix of review talks, introducing members of the group to the underlying technologies of the CRASH center, and specific students speaking about their research. In addition, students were involved in 20 of the posters presented at the annual review.

The primary educational effort this year has been on course development. In the fall semester, a new course was offered at TAMU. Its emphasis was on verification, validation, sensitivity analysis and uncertainty quantification. Prof. Ryan McClarren was the lead instructor; he developed and offered the course, with 10 students from a number of departments in attendance. In the winter semester, a new course was also taught at Michigan. It was team-taught by Profs. James Holloway, Vijay Nair and Ken Powell. It focused on input/output modeling, screening and sensitivity analysis and uncertainty quantification. Students developed a simple simulation code, and exercised some basic uncertainty quantification and sensitivity analysis on that code. In the latter half of the semester, students applied the techniques they learned in the course to simulation codes they were using in their research. Twenty students attended the course. Several of these students, and several from outside the CRASH project, are enrolled in the Scientific Computing certificate program. This program requires several courses in numerical methods, several courses in computer science, in addition to the requirements for the PhD in the student's home department. Some of the CRASH students enrolled in the certificate program are pursuing the Predictive Science track of the Scientific Computing certificate.

VI. Graduate Student Research

Computational and Statistical Students:

Eric Baker and his PhD advisor Edward Larsen have been developing a model for simulating radiation transport in a system that is so geometrically complex that it can be understood as "random." Currently, the only available method for such systems is the "atomic mix" method, in which the material cross sections (opacities) are volume-averaged. The atomic mix method is accurate when the "chunks" of the two (or more) materials are optically thin, but not when the chunks are not thin, and it has been a long-standing problem to obtain a simple but accurate model for radiation transport in such random-media problems. The research that Eric is doing is based on a recent PhD project by another of Prof. Larsen's students, in which the transport equation is replaced by a more complex equation in which the distribution function for distance to collision is not

exponential. This non-exponential distribution function is obtained by sampling the random histories of a large number of Monte Carlo particles in a large number of realizations of the random system. That previous work was successful; now Eric is attempting to simplify the method so that it can be more easily used in practical problems. Eric's results so far are limited to 1-D, but are promising.

Three-dimensional radiation transport calculations with moderately good spatial, angular, and energy resolution remain challenging even on modern supercomputers. This will limit the number of high-fidelity calculations that will be possible. Thus, every increase in efficiency (accuracy per unit computational resource) will increase the value of the transport capability to the project. One way to increase efficiency is to make the required iterations converge more rapidly, and one proven way to do this is to use a diffusion-based preconditioner. **Anthony Barbu** has devised a particularly efficient diffusion-based preconditioner that he has shown to be effective given transport discretizations of the type used in PDT. [Reference: A. P. Barbu and M. L. Adams, "Semi-Consistent Diffusion Synthetic Acceleration for Discontinuous Discretizations of Transport Problems," Proc. Intl. Conf. on Mathematics, Computation, and Reactor Physics, Saratoga Springs, NY, May 3-7 (2009). CD-ROM.] He is now implementing this preconditioner in the PDT code.

Dr. Jesse Cheatham (now graduated and working at Oak Ridge National Laboratory) has provided a detailed and systematic investigation of the time truncation error in the Implicit Monte Carlo (IMC) and Carter-Forrest (CF) methods of radiative transfer Monte Carlo. This work has led to the identification of the leading source of truncation error for both the IMC and CF methods. This analysis suggests that by applying a predictor-corrector to estimate the opacity at the middle of the time step, the CF method can be made a second order accurate method in nonlinear problems. Dr. Cheatham's work has also examined the spatial discretization error known as photon teleportation and shown that a maximum-entropy functional expansion tally can be used to reduce this source of error. The temporal truncation analysis has also suggested a new time-step controller for radiative transfer problems, based on controlling the change in the opacity during a time step.

Jason Chou has been a key player in the one-dimensional uncertainty quantification analysis of the CRASH code during the past year. He has developed automatic software pipelines for handling large numbers of simulations for both the shock tube and the CRASH experiment simulations and has developed feature extraction algorithms for both cases. He has also carried out resolution studies and variable screening to help determine the appropriate parameter space to explore for the 1D CRASH UQ study. Recently, he has been looking into the generation of unphysical oscillations at material interfaces when hydrodynamics is coupled with gray diffusion and its potential role in producing artifacts in multidimensional simulations.

Dr. Greg Davidson and his PhD advisor Edward Larsen have developed a new "Staggered Block Jacobi" (SBJ) method for time-discretizing the Boltzmann transport equation which (i) does not require sweeps, (ii) is unconditionally stable, (iii) is highly

accurate for optically thick, diffusive problems, (iv) is trivially parallel, and (v) allows for multiphysics simulations without an operator split. Greg developed the SBJ method, and he encoded and tested it for linear 1-D "neutron" transport problems and nonlinear 1-D thermal radiation transport problems. The SBJ method is highly accurate for optically thick systems in which radiation waves travel only through a fraction of a cell during a time step. However, for problems containing optically thin subsystems, in which radiation travels long distances during a time step, the method becomes less accurate unless extremely small time steps are used. Overall, the new SBJ method complements the current well-known sweep-based methods, which are (i) not easily parallelized, (ii) efficient for optically thin systems, (iii) problematic for optically thick systems, and (iv) require time-splitting for multiphysics simulations. Greg defended his PhD in December, 2009. He is now a staff scientist at Oak Ridge National Laboratory.

Over the last year, **Jarrold Edwards** has performed a study relating to the application of the Trapezoidal/BDF-2 time discretization scheme to non-linear radiation diffusion. The trapezoidal/BDF-2 method offers several advantages over more commonly known second-order schemes such as the Crank-Nicholson scheme, the BDF-2 scheme, and the linear discontinuous-Galerkin scheme. We have defined several non-linear variants of the Trapezoidal/BDF-2 scheme and compared their performance on a set of test problems. An article on this work is now being prepared for submittal to the Journal of Computational Physics. Once this article has been completed, Jarrod will begin applying the trapezoidal/BDF-2 method within an IMEX method (a multiphysics solution technique based upon a combination of explicit and implicit time integration) for solving the radiation-hydrodynamics equations.

A significant challenge in many UQ efforts, including that of CRASH, is how to handle large numbers of uncertain inputs such as EOS relations and opacities (which depend on temperature, density, and frequency). One goal of CRASH is to develop, employ, and evaluate methods for dimension reduction in such cases. **Adam Hetzler** is working under the direction of M. L. Adams and R. McClarren to tackle dimension reduction for the opacities that are currently being generated by I. Sokolov. In Sokolov's model these opacities depend on models of the state of the plasma but also on ionization potentials and excitation energies, which are themselves uncertain. The ultimate goal of dimension reduction for opacities will exploit the dependence of the uncertainties of the model's opacities on the uncertainties in ionization potentials and excitation energies. Adam is working to characterize this dependence. Dimension reduction may also exploit correlations among the large set of numbers that characterize a material's opacity -- correlations that are buried in Sokolov's model. This we expect to address later.

Kwok Ho (Marcus) Lo is a doctoral candidate in Aerospace Engineering, advised by Prof. Bram van Leer. He is expected to defend his dissertation in April 2010. His research project is the development of a space-time discontinuous Galerkin code for the Navier-Stokes equations. The code makes use of the principle of "recovery" developed Van Leer and collaborators since 2004. This principle replaces a discontinuous discretization with a higher-order smooth representation that has the same L2 projection on the contributing meshes. The space-time marching scheme is a nontrivial extension of Hancock's

predictor-corrector scheme for the Euler equations; it is significantly more efficient than its competitor, the Space Time Extension (STE) method of C.-D. Munz et al. Much of the dissertation is dedicated to the accuracy and stability analysis of the underlying linear scheme on regular and irregular grids.

Over the past year, **Colin Miranda** has been studying and implementing uncertainty quantification (UQ) algorithms that incorporate adjoint solutions for improved efficiency. Existing UQ algorithms based on stochastic expansion and response surface generation rely only on scalar output values and hence become expensive for large input dimensions or order expansions. Adjoint solutions provide output gradients as well as values, and this extra information can significantly improve the accuracy of the constructed response surfaces. However, making use of this gradient information is not trivial when the dimension of the input space is large or when non-tensor product sampling is employed. To this end, Colin has identified six multi-variate interpolation techniques into which gradient information can be incorporated. He has implemented each of them in multiple dimensions, and he has analyzed their performance for an analytic input-to-output model. He has documented the implementation, advantages, and disadvantages of each method in a report. The next step will be to submit this report to a journal as a review publication. In addition, Colin will work on applying the modified UQ algorithms to a radiation-hydrodynamics test case, using a discontinuous Galerkin solver with adjoint capability.

Tiberius Moran-Lopez (Ph.D. candidate) Is exploring the effects of turbulence on radiative gas dynamics. Preliminary work is to analyze a self-similar Taylor-Sedov blast wave with turbulence described by a $K-\epsilon$ turbulence model. Parameters of interest are the gas density, velocity, pressure, radiation energy density and flux, turbulent kinetic energy, and its dissipation rate. The self-similar solution satisfies a system of implicitly defined nonlinear ODEs, the solution of which is being investigated through an iteration on second derivatives in the ODEs (which arise only because of turbulent effects) and the turbulent terms in the boundary conditions at the shock. Potential applications of these studies include astrophysical events, inertial confinement fusion (IFC), and high energy density phenomena.

Ashin Mukherjee is a second year PhD student in Statistics. He is still working on developing a thesis research topic. It is expected that he will work with Professor Nair and Associate professor Ji Zhu. Ashin has also been providing data analysis support for the UQ research team, fitting MARS, MART and other models to the computer experiment data. He is also providing support to Professors Holloway, Powell and Nair in the new UQ course that they are teaching.

Nick Patterson (advisor: Thornton) has worked on automatic feature detection algorithms over the past eight months, He succeeded in developing Matlab and IDL programs that identify the shock front, wall positions, and the kink location in both experimental and simulated radiographs, as well as the wall shock for the simulated radiographs. He is now moving onto his thesis project on radiative transfer in heterogeneous media.

Dave Starinshak (Mathematics) has been working on numerical discretization aspects of compressible multimaterial flow models using level-sets. It is well-known that naive discretization schemes may generate non-physical oscillations across material fronts, and consequently may trigger physical instabilities and false dynamics in multidimensional flow. By now, there are various established strategies to circumvent these oscillations in pure multimaterial fluid dynamics set-up. Dave is looking to extend these ideas to flow models that also include radiation energy equation with gray diffusion and an energy-exchange source term coupling matter and radiation. We currently use a simplified 1D model that we hope retains the main computational issues observed in the full 3D CRASH code, and try to understand the additional difficulties due to radiation energy and energy-exchange terms. We also work on extending current two-material algorithms to flows consisting of three fluid components, in the spirit of CRASH, and study strategies for implementing level sets to track material fronts in this context.

Methodologies for uncertainty quantification (UQ) and predictions are becoming more complicated and are being used to support high-consequence decisions. It is important to assess how accurately these methods quantify uncertainty and make predictions. For example, if a methodology claims that one can predict a certain class of outputs to within 10% of reality, how does one know that this figure is meaningful? How does one know that a given UQ methodology does not systematically under- or over-predict uncertainties? **Hayes Stripling** is working under the direction of M. L. Adams and in collaboration with P. Dykema of LLNL to develop and employ a "method of manufactured universes" (MMU) to assess methodologies and software such as the Kennedy-O'Hagan model and its embodiment in software from the LANL statistics group. MMU works as follows:

1. Define laws that govern the manufactured universe. This means creating mathematical models that define the laws and constants that go into the models.
2. Create "experiments" by defining physical problems and using the manufactured laws to create exact output quantities of interest (QOIs). Then create "measured data" by perturbing these output QOIs using an error model, if desired.
3. Define an approximate model on which the UQ methodology is to be tested. (For example, this could be grey diffusion if the manufactured reality is multi-frequency Boltzmann.)
4. Define approximate physical constants and prior estimates of uncertainties. These will serve as uncertain inputs in the test. (An interesting case would be testing how various UQ methodologies behave when input-parameter uncertainties are over- or under-estimated.)
5. Apply the given methodology to the collection of {approximate model, uncertain input constants, uncertain measured data}.
6. Define a new set of experimental problems and predict the values of the new QOIs, using what was learned from the given methodology. The methodology should give an estimate for how closely the predictions should match the real measured data.
7. Generate the "real" new QOIs, using the manufactured laws, and new "measured data," using measurement-error models if desired, and compare against the predictions.

8. Develop and apply metrics to quantify how well the given methodology performed.
9. Repeat with variations on approximate models, measurement-error models, “data” uncertainties, UQ methodology, and universal laws.
10. Determine when and why existing methodologies fail and devise improvements.

Dan Zaide has been researching basic algorithm advances for flows related to the CRASH problem. He has worked jointly with another CRASH graduate student (Tiberius Moran-Lopez) on incorporating turbulence models into radiative shock modeling; this work was done in collaboration with Oleg Schilling of LLNL, and was presented at the APS fluids meeting in November of 2009. Dan has also looked at ways to improve Lagrangian methods for multi-fluid flows, leading to a presentation (with Prof. Phil Roe) at a Multi-Material Fluids and Structures meeting. Dan's primary work has been adding rad-hydro capabilities (based on a P1 closure) to a Discontinuous Galerkin code developed by Prof. Chris Fidkowski.

Zach Zhang is a 3rd year PhD student in the Statistics Department. He is working with Professor Vijay Nair and Associate Professor Ji Zhu on his dissertation. He was advanced to candidacy over the past year. His thesis research involves studying both Bayesian and frequentist methods for modeling and analyzing the outputs of computer models in large-scale simulation experiments and combining them with field data. In particular, over the past few months, he has been studying the calibration problem and has obtained some results connecting the frequentist spline-based methods and the Bayesian methods. He has developed a pseudo-likelihood approach for estimating the calibration parameter that appears to be computationally faster than the Bayesian approach. In addition, he has also been providing data analysis support for the UQ research team. He is currently helping Professors Holloway, Powell and Nair in the new UQ course that they are teaching.

Experimental Students

The research of the experimental graduate students is supported at least in part by CRASH, but also by the Stewardship Sciences Academic Alliances program and the National Laser User Facility program, both funded by Defense Sciences within NNSA.

Graduate student **Forrest Doss** is continuing work begun by Dr. Amy Reighard Cooper, now employed by LLNL and doing shots on NIF. Amy developed the radiative shock experimental platform that is the basis for much of our further work with radiative shocks. This platform uses Omega to irradiate a Be disk for 1 ns at $\sim 7 \times 10^{14}$ W/cm², accelerating the Be to above 100 km/s and launching a shock into a gas-filled shock tube at an initial velocity near 200 km/s. Using Xe or Ar gas creates a radiative shock, in which radiation from the shocked material heats the upstream layer. The energy loss from the shocked layer in turn leads to a large increase in its density. In the Xe case, the shocked layer becomes optically quite thick to the thermal radiation (at near 50 eV). Amy published a number of papers describing her work to develop this system and initial observations of it.⁹⁻¹² Some additional papers related mainly to the theory of such systems were published by Prof. Drake and collaborators.¹³⁻¹⁵ Amy's work set the context in

which we were able to obtain funding for the Center for Radiative Shock Hydrodynamics (CRASH), which is greatly increasing our ability to support similar experiments with multi-dimensional modeling and has partially supported the work described below.

Forrest Doss was subsequently challenged to understand the many interesting details that can be seen in the radiographs of the radiative shocks in Xe. These are illustrated in Figure 37. Forrest has made great progress in this. He was the person who identified the features labeled in Figure 33 as wall shocks, produced when radiation from the primary shock ablates the walls of the shock tube. He did this first by examining Amy's radiographs in the context of simulations he was doing using HYDRA. He then obtained improved data like that shown in the figure, in which the wall shocks are very evident, and published the results.³ He also has published an analysis of the reproducibility of the properties that may be observed in the radiographs.⁵ In the radiographs, one can see structure in the dense Xe layer that is probably related to a variant of the Vishniac instability, well known to cause modulations in thin, expanding astrophysical shells. Forrest has just resubmitted his paper² on the theory of the modified instability to the *Astrophysical Journal*, and is continuing experiments to attempt to find clearer evidence of it.

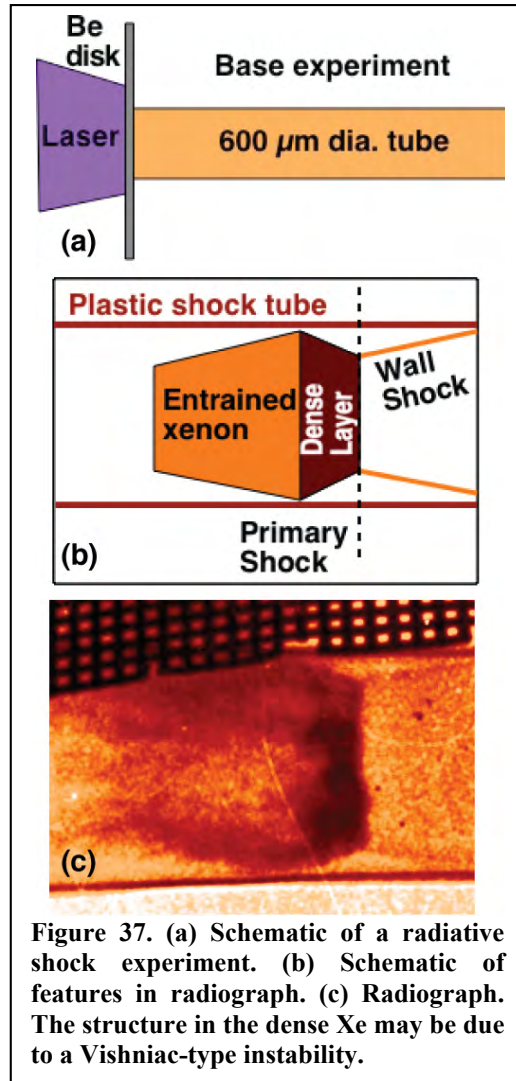


Figure 37. (a) Schematic of a radiative shock experiment. (b) Schematic of features in radiograph. (c) Radiograph. The structure in the dense Xe may be due to a Vishniac-type instability.

Graduate student **Tony Visco** was challenged to better diagnose the Ar-gas variant of this type of system (where features are spread out enough that one can hope to diagnose them). He has done experiments at Omega that used UV Thomson scattering, streaked optical pyrometry, and x-ray Thomson scattering to diagnose these plasmas. He is now analyzing data and working on papers reporting the results. Tony also participated in some measurements to understand spectrometer behavior with short laser pulses, which led to a publication.¹⁶

Graduate student **Channing Huntington** was asked to further advance x-ray Thomson scattering techniques, and has been developing methods to enable us to more distinctly determine the spatial profiles of temperatures and ionization in the radiative shocks with Xe gas. He performed some experiments on Omega in 2009 and will again be shooting in March 2010. Chan, with graduate student **Christine Krauland**, also developed and is publishing⁶ an analysis of imaging x-ray scattering as a diagnostic technique. We have

very high hopes for this technique in the NIF context. It remains to be seen whether we can get enough x-rays from Omega to make it effective there. Chan also did some experiments on the high-intensity HERCULES laser at Michigan, in collaboration with Karl Krushelnick's group, which should lead to at least one publication. Christine is now developing an experimental design for an experiment with colliding radiative shocks, which should push us to much-higher-density shocked matter. We have hopes that this will develop into a novel direction for future research. First-year graduate student **Rachel Young**, who has an interest in design, will be using the CRASH code to contribute multi-dimensional modeling of these potential experiments.

Graduate student **Eliseo Gamboa** has a significant interest in instrumentation. We have teamed him with David Montgomery at LANL to develop and use an imaging x-ray spectrometer for imaging x-ray Thomson spectroscopy. His ultimate goal is to develop a system that can effectively be fielded through one diagnostic inserter (TIM) on Omega. This will enable one to obtain well-resolved spatial profiles of temperature and ionization, and will be useful to a very wide range of experiments in addition to our work with radiative shocks. Eliseo's initial graduate student project involved the completion of a system for directly measuring the charge bunches produced by microchannel plates. This system will allow a more definite understanding of the noise properties of x-ray images produced using microchannel-plate intensifiers. He will be submitting a paper to *Reviews of Scientific Instruments* this spring. This continues our long-term exploration of these devices, which previously led to a publications by Eric Harding¹⁷ on optical pulse height measurements and modeling and by an undergraduate student¹⁸ on the use of transmission photocathodes with them.

Our nonlinear hydrodynamics thrust has included work on instabilities driven by blast waves like those produced when supernovae explode, and work to observe the Kelvin-Helmholtz instability under high-energy density conditions. **Dr. Carolyn Kuranz** completed her thesis work by making significant advances in our measurement techniques and experimental understanding of the blast-wave-driven case. Her work on measurements led to very substantial improvements in the quality of our radiographic data in all contexts.¹⁹⁻²¹ She also realized that there are wall shocks in our hydrodynamic experiments, produced by early effects of the laser-plasma interactions, and used these to obtain an estimate of the early heating of the shock-tube walls.²² In addition, we participated in a study to explore the effect of increased preheat using the front-tracking code FronTier²³. Carolyn has published a sequence of experiments in which the initial conditions for the blast-wave-driven instabilities were varied, in an experiment scaled to the explosion dynamics of a well-known supernova (SN 1987A). These experiments^{24,25} and related simulations³⁰⁻²⁸ showed that some of our preconceptions about the impact of varying the initial conditions were not correct. Carolyn also observed that the morphology of the spikes of dense material penetrating the less-dense material has a number of mysterious features.²⁹ These mysterious features are potentially related to magnetic-field generation within these targets,³⁰ among other possibilities. In work going on now, junior graduate student **Carlos DiStefano** is experimentally investigating these features both by varying the target properties and by doing experiments that can detect magnetic fields if they are present. In a related effort, we developed and published³¹ a

design for a NIF experiment on blast-wave-driven instabilities, in which it will be possible to use a diverging system with two interfaces, with the masses of various layers scaled to those in the pre-supernova star.

VII. References

- ¹ T.R. Boehly, R.S. Craxton, T.H. Hinterman, J.H. Kelly, T.J. Kessler, S.A. Kumpman, S.A. Letzring, R.L. McCrory, S.F.B. Morse, W. Seka, S. Skupsky, J.M. Soures, and C.P. Verdon, The upgrade to the OMEGA laser system, *Rev. Sci. Instr.* 66, 508 (1995).
- ² F.W. Doss, R.P. Drake, and H.F. Robey, Early-time stability of decelerating shocks, *Astrophysical Journal*, submitted (2009).
- ³ F.W. Doss, H.F. Robey, R.P. Drake, and C.C. Kuranz, Wall shocks in high-energy-density shock tube experiments, *Physics Of Plasmas* 16, 112705 (2009).
- ⁴ C. Michaut, E. Falize, C. Cavet, S. Bouquet, M. Koenig, T. Vinci, A. Reighard, and R. P. Drake, Classification of and recent research involving radiative shocks, *Astrophysics and Space Science* 322, 77 (2009).
- ⁵ F.W. Doss, R.P. Drake, and H.F. Robey, Repeatability in radiative shock tube experiments, *High Energy Density Physics*, doi:10.1016/j.hedp.2009.12.007 (2010).
- ⁶ C.M. Huntington, C.C. Krauland, C. C. Kuranz, S.H. Glenzer, and R. P. Drake, Imaging Scattered X-Ray Radiation for Measurement of Local Electron Density in High-Energy-Density Experiments, *High Energy Density Physics*, in press (2010).
- ⁷ R.G. McClarren and R. P. Drake, Radiative Transfer In the Cooling Layer of a Radiating Shock, *Journal of Quantitative Spectroscopy and Radiative Transfer*, submitted (2010).
- ⁸ R. B. Lowrie and J. D. Edwards, Radiative shock solutions with grey nonequilibrium diffusion, *Shock Waves* 18, 129 (2008).
- ⁹ A.B. Reighard, R. P. Drake, K.K. Dannenberg, D. J. Kremer, E.C. Harding, D.R. Leibbrandt, S.G. Glendinning, T.S. Perry, B.A. Remington, J. Greenough, J. Knauer, T. Boehly, S. Bouquet, L. Boireau, M. Koenig, and T. Vinci, Collapsing radiative shocks in xenon on the Omega laser, *Phys. Plas.* 13, 082901 (2006).
- ¹⁰ A.B. Reighard, R.P. Drake, T. Donjakowski, M.J. Grosskopf, K.K. Dannenberg, D. Froula, S. Glenzer, J.S. Ross, and J. Edwards, Thomson Scattering from a shock front, *Rev. Sci. Instr.* 77, 10E504 1 (2006).
- ¹¹ A.B. Reighard, R. P. Drake, J.E. Mucino, J.P. Knauer, and M. Busquet, Planar radiative shock experiments and their comparison to simulations, *Phys. Plas.* 14, 056504 (2007).
- ¹² A.B. Reighard and R.P. Drake, The formation of a cooling layer in a partially optically thick shock, *Astrophysics and Space Science* 307, 121 (2007).
- ¹³ R. P. Drake and A. B. Reighard, Theory and experiment on radiative shocks, *Shock Compression of Condensed Matter*, AIP Conference Proceedings, in press (2006).

- 14 R.P. Drake, Theory of radiative shocks in optically thick media, *Phys. Plasmas* 14, 043301 (2007).
- 15 R.P. Drake, Energy balance and structural regimes of radiative shocks in optically thick media, *IEEE Transactions on Plasma Science* 35, 171 (2007).
- 16 A. Visco, R.P. Drake, D.H. Froula, S.H. Glenzer, and B.B. Pollock, Temporal dispersion of a spectrometer, *Review Of Scientific Instruments* 79, 10F545 (2008).
- 17 E.C. Harding and R.P. Drake, A 3D model of x-ray induced microchannel plate output, *Rev. Sci. Inst.* 77, 10E312 1 (2006).
- 18 M.E. Lowenstern, E.C. Harding, C. Huntington, A.J. Visco, and R.P. Drake, Performance of Au Transmission Photocathode on a Microchannel Plate Detector, *Review Of Scientific Instruments* 79, 10E912 (2008).
- 19 C. C. Kuranz, B. E. Blue, R.P. Drake, H.F. Robey, J.F. Hansen, J.P. Knauer, M.J. Grosskopf, C. Krauland, and D.C. Marion, Dual, orthogonal, backlit pinhole radiography in Omega experiments, *Rev. Sci. Inst.* 77, 10E327 1 (2006).
- 20 C.C. Kuranz, R.P. Drake, T.L. Donajkowski, K.K. Dannenberg, M. Grosskopf, D.J. Kremer, C. Krauland, D.C. Marion, H.F. Robey, B.A. Remington, J.F. Hansen, B.E. Blue, J. Knauer, T. Plewa, and N. Hearn, Assessing mix layer amplitude in 3D decelerating interface experiments, *Astrophysics and Space Science* 307, 115 (2007).
- 21 C.C. Kuranz, R.P. Drake, M.J. Grosskopf, H.F. Robey, B.A. Remington, J.F. Hansen, B.E. Blue, and J.P. Knauer, Image processing of radiographs in 3D Rayleigh-Taylor decelerating interface experiments, *Astrophysics and Space Science* 322, 45 (2009).
- 22 C.C. Kuranz, F.W. Doss, R.P. Drake, M.J. Grosskopf, and H.F. Robey, Using wall shocks to measure preheat in laser-irradiated, high-energy-density, hydrodynamics experiments, *High Energy Density Physics*, in press (2010).
- 23 Yongmin Zhang, R.P. Drake, and James Glimm, Numerical evaluation of impact of laser preheat on interface structure and stability, *Phys. Plas.* 14, 062703 (2007).
- 24 C.C. Kuranz, R.P. Drake, E.C. Harding, M.J. Grosskopf, H. F. Robey, B.A. Remington, M.J. Edwards, A.R. Miles, T.S. Perry, T. Plewa, N.C. Hearn, J.P. Knauer, D. Arnett, and D.R. Leibbrandt, Two-dimensional blast-wave-driven Rayleigh-Taylor instability: experiment and simulation, *Astrophysical Journal* 696, 749 (2009).
- 25 C.C. Kuranz, R.P. Drake, M.J. Grosskopf, A. Budde, C. Krauland, D.C. Marion, A.J. Visco, J.R. Ditmar, H. F. Robey, B.A. Remington, A.R. Miles, A.B.R. Cooper, C. Sorce, T. Plewa, N.C. Hearn, K.L. Killibrew, J.P. Knauer, D. Arnett, and T. Donajkowski, Three-dimensional blast-wave-driven Rayleigh-Taylor instability and the effects of long-wavelength modes, *Physics Of Plasmas* 16, 156310 (2009).
- 30 N. Hearn, T. Plewa, R.P. Drake, and C.C. Kuranz, FLASH code simulations of Rayleigh-Taylor and Richtmyer-Meshkov instabilities in laser-driven experiments, *Astrophysics and Space Science* 307, 227 (2007).
- 27 N.C. Hearn, T. Plewa, R.P. Drake, and C.C. Kuranz, Flash code simulations of laser-driven Rayleigh-Taylor and Richtmyer-Meshkov Experiments on Omega, in *Proceedings of the Tenth International Workshop on The Physics of Compressible*

Turbulent Mixing, edited by M. Legrand and M. Vandenboomgaerde (Commissariat a l'Energie Atomique, Bruyeres-le-Chatel, 2007), pp. 114.

28 A. Budde, R. P. Drake, C. C. Kuranz, M.J. Grosskopf, T. Plewa, and N.C. Hearn, Simulation of fabrication variations in supernova hydrodynamics experiments, High Energy Density Physics, submitted (2010).

29 C.C. Kuranz, R.P. Drake, M.J. Grosskopf, B. Fryxell, A. Budde, J.F. Hansen, A.R. Miles, T. Plewa, N.C. Hearn, and J.P. Knauer, Spike morphology in blast-wave-driven instability experiments, Physics of Plasmas, submitted (2009).

30 B. Fryxell, C. C. Kuranz, R. P. Drake, M.J. Grosskopf, A. Budde, T. Plewa, J. F. Hansen, A. R. Miles, and J. Knauer, The Possible Effects of Magnetic Fields on Laser Experiments of Rayleigh-Taylor Instabilities, High Energy Density Physics, in press (2010).

31 M. J. Grosskopf, R. P. Drake, C. C. Kuranz, A. R. Miles, J. F. Hansen, T. Plewa, N. Hearn, D. Arnett, and J. C. Wheeler, Modeling of multi-interface, diverging, hydrodynamic experiments for the National Ignition Facility, Astrophysics and Space Science 322, 57 (2009).